

1 **TMPRSS2 and furin are both essential for proteolytic activation and spread of SARS-
2 CoV-2 in human airway epithelial cells and provide promising drug targets**

3
4
5 Dorothea Bestle^{1#}, Miriam Ruth Heindl^{1#}, Hannah Limburg^{1#}, Thuy Van Lam van², Oliver
6 Pilgram², Hong Moulton³, David A. Stein³, Kornelia Hardes^{2,4}, Markus Eickmann^{1,5}, Olga
7 Dolnik^{1,5}, Cornelius Rohde^{1,5}, Stephan Becker^{1,5}, Hans-Dieter Klenk¹, Wolfgang Garten¹,
8 Torsten Steinmetzer², and Eva Böttcher-Friebertshäuser^{1*}

9
10 1) Institute of Virology, Philipps-University, Marburg, Germany
11 2) Institute of Pharmaceutical Chemistry, Philipps-University, Marburg, Germany
12 3) Department of Biomedical Sciences, Carlson College of Veterinary Medicine, Oregon
13 State University, Corvallis, USA
14 4) Fraunhofer Institute for Molecular Biology and Applied Ecology, Gießen, Germany
15 5) German Center for Infection Research (DZIF), Marburg-Gießen-Langen Site, Emerging
16 Infections Unit, Philipps-University, Marburg, Germany

17
18 #These authors contributed equally to this work.

19
20 *Corresponding author: Eva Böttcher-Friebertshäuser
21 Institute of Virology, Philipps-University Marburg
22 Hans-Meerwein-Straße 2, 35043 Marburg, Germany
23 Tel: 0049-6421-2866019
24 E-mail: friebertshaeuser@staff.uni-marburg.de

25
26 Short title: TMPRSS2 and furin activate SARS-CoV-2 spike protein

27
28

29 **Abstract (295)**

30 In December 2019, a novel coronavirus named SARS-CoV-2 first reported in Wuhan, China,
31 emerged and rapidly spread to numerous other countries globally, causing the current
32 pandemic. SARS-CoV-2 causes acute infection of the respiratory tract (COVID-19) that can
33 result in severe disease and lethality. Currently, there is no approved antiviral drug for
34 treating COVID-19 patients and there is an urgent need for specific antiviral therapies and
35 vaccines.

36 In order for SARS-CoV-2 to enter cells, its surface glycoprotein spike (S) must be cleaved at
37 two different sites by host cell proteases, which therefore represent potential drug targets. In
38 the present study we investigated which host cell proteases activate the SARS-CoV-2 S
39 protein in Calu-3 human airway epithelial cells. We show that S can be cleaved by both the
40 proprotein convertase furin at the S1/S2 site and the transmembrane serine protease 2
41 (TMPRSS2) at the S2' site. We demonstrate that TMPRSS2 is essential for activation of
42 SARS-CoV-2 S in Calu-3 cells through antisense-mediated knockdown of TMPRSS2
43 expression. Further, we show that SARS-CoV-2 replication can be efficiently inhibited by two
44 synthetic inhibitors of TMPRSS2 and also by the broad range serine protease inhibitor
45 aprotinin. Additionally, SARS-CoV-2 replication was also strongly inhibited by the synthetic
46 furin inhibitor MI-1851. Combining various TMPRSS2 inhibitors with MI-1851 produced more
47 potent antiviral activity against SARS-CoV-2 than an equimolar amount of any single serine
48 protease inhibitor. In contrast, inhibition of endosomal cathepsins by E64d did not affect virus
49 replication.

50 Our data demonstrate that both TMPRSS2 and furin are essential for SARS-CoV-2 activation
51 in human airway cells and are promising drug targets for the treatment of COVID-19 either by
52 targeting one of these proteases alone or by a combination of furin and TMPRSS2 inhibitors.
53 Therefore, this approach has a high therapeutic potential for treatment of COVID-19.

54

55 **Introduction**

56 In December 2019, a new coronavirus (CoV) emerged which rapidly spreads around the
57 world causing a pandemic never observed before with these viruses. The virus was identified
58 as a new member of the lineage b of the genus *Betacoronavirus* that also contains the 2002
59 severe acute respiratory syndrome (SARS)-CoV and was named SARS-CoV-2 by the WHO.
60 The respiratory disease caused by the virus was designated as coronavirus disease 2019
61 (COVID-19).

62 CoVs are a large family of enveloped, single-stranded positive-sense RNA viruses belonging
63 to the order *Nidovirales* and infect a broad range of mammalian and avian species, causing
64 respiratory or enteric diseases. CoVs have a major surface protein, the spike (S)
65 protein, which initiates infection by receptor binding and fusion of the viral lipid envelope with
66 cellular membranes. Like fusion proteins of many other viruses, the S protein is activated by
67 cellular proteases. Activation of CoV S is a complex process that requires proteolytic
68 cleavage of S at two distinct sites, S1/S2 and S2' (Fig. 1), generating the subunits S1 and S2
69 that remain non-covalently linked (Belouzard et al. 2009; Follis et al. 2006; Bosch et al.,
70 2008). The S1 subunit contains the receptor binding domain, while the S2 subunit is
71 membrane-anchored and harbours the fusion machinery. Cleavage at the S2' site, located
72 immediately upstream of the hydrophobic fusion peptide, has been proposed to trigger the
73 membrane fusion activity of S (Madu et al., 2009; Walls et al., 2016). In contrast, the
74 relevance of S cleavage at the S1/S2 site is yet not fully understood. Processing of CoV S is
75 believed to occur sequentially, with cleavage at the S1/S2 site occurring first and subsequent
76 cleavage at S2'. Cleavage at the S1/S2 site may be crucial for conformational changes
77 required for receptor binding and/or subsequent exposure of the S2' site to host proteases at
78 the stage of entry (reviewed in Head-Sargent and Gallagher, 2012; Millet and Whittaker,
79 2015; Hoffmann et al., 2018).

80 Many proteases have been found to activate CoVs *in vitro* including furin, cathepsin L, and
81 trypsin-like serine proteases such as the transmembrane serine protease 2 (TMPRSS2),
82 TMPRSS11A, and TMPRSS11D (reviewed in Head-Sargent and Gallagher, 2012; Millet and
83 Whittaker, 2015; Hoffmann et al., 2018). Among them, TMPRSS2 and furin play major roles
84 in proteolytic activation of a broad range of viruses (reviewed in Klenk and Garten, 1994;
85 Garten, 2018; Böttcher-Friebertshäuser, 2018). TMPRSS2 is a type II transmembrane serine
86 protease (TTSP) that is widely expressed in epithelial cells of the respiratory, gastrointestinal
87 and urogenital tract (reviewed in Bugge et al., 2009; Böttcher-Friebertshäuser, 2018). The
88 physiological role of TMPRSS2 is yet unknown, but TMPRSS2-deficient mice lack a
89 discernible phenotype suggesting functional redundancy (Kim et al., 2006). In 2006, we first
90 identified TMPRSS2 as a virus activating protease, by demonstrating that it cleaves the

91 surface glycoprotein hemagglutinin (HA) of human influenza A viruses (Böttcher et al., 2006).
92 Subsequently, TMPRSS2 was shown to activate the fusion proteins of a number of other
93 respiratory viruses including human metapneumovirus, human parainfluenza viruses as well
94 as CoVs including SARS-CoV and Middle East respiratory syndrome (MERS)-CoV in vitro
95 (reviewed in Böttcher-Friebertshäuser, 2018; Hoffmann et al., 2018). TMPRSS2 cleaves at
96 single arginine or lysine residues (R/K↓), and hence, activates viral fusion proteins at so
97 called monobasic cleavage sites. More recent studies by us and others demonstrated that
98 TMPRSS2-deficient mice do not suffer from pathology when infected with certain influenza A
99 virus strains, SARS-CoV and MERS-CoV, respectively, due to inhibition of proteolytic
100 activation of progeny virus and consequently inhibition of virus spread along the respiratory
101 tract (Hatesuer et al., 2013; Tarnow et al., 2014; Sakai et al., 2014; Iwata-Yoshikawa et al.,
102 2019). These studies identified TMPRSS2 as an essential host cell factor for these
103 respiratory viruses and further demonstrated that inhibition of virus activating host cell
104 proteases, particularly TMPRSS2, provides a promising approach for the development of
105 therapeutics to treat respiratory virus infections. The proprotein convertase (PC) furin is a
106 type I transmembrane protein that is ubiquitously expressed in eukaryotic tissues and cells.
107 Furin cleaves the precursors of a broad range of proteins including hormones, growth
108 factors, cell surface receptors and adhesion molecules during their transport along the
109 secretory pathway at multibasic motifs of the preferred consensus sequence R-X-R/K-R↓
110 (reviewed in Garten, 2018). Moreover, furin has been identified as an activating protease for
111 the fusion proteins of a broad range of viruses including highly pathogenic avian influenza A
112 viruses (HPAIV), human immunodeficiency virus (HIV), Ebola virus, Measles virus, and
113 Yellow Fever virus as well as bacterial toxins such as Shiga toxin or anthrax toxin at
114 multibasic motifs (reviewed in Klenk and Garten, 1994; Rockwell et al., 2002; Garten, 2018).
115 Acquisition of a multibasic cleavage site by insertion of basic amino acids has long been
116 known to be a prime determinant of avian influenza A virus pathogenicity in poultry.
117 Activation of the surface glycoprotein HA of HPAIV by furin supports systemic spread of
118 infection with often lethal outcome. In contrast, the HA of low pathogenic avian influenza A
119 viruses (LPAIV) is activated at a monobasic cleavage site by trypsin-like serine proteases.
120 Appropriate proteases are believed to be expressed in the respiratory and intestinal tract of
121 birds, confining spread of infection to these tissues.

122 A recent study by Hoffmann et al. indicates that TMPRSS2 is also involved in SARS-CoV-2 S
123 protein activation (Hoffmann et al., 2020). The authors show that transient expression of
124 TMPRSS2 in Vero cells supports cathepsin-independent entry of SARS-CoV-2 pseudotypes.
125 Moreover, pretreatment of human Caco-2 colon and human airway cells with the broad range
126 inhibitor camostat mesylate that also inhibits TMPRSS2 activity, markedly reduced entry of
127 SARS-CoV-2 as well as VSV pseudotypes containing the SARS-CoV-2 S protein. This

128 indicates that a trypsin-like serine protease is crucial for SARS-CoV-2 entry into these cells.
129 However, sequence analysis of the SARS-CoV-2 S protein suggests that furin may also be
130 involved in S processing (Fig. 1B; Coutard et al., 2020; Walls et al., 2020). The S1/S2 site of
131 SARS-CoV-2 S protein contains an insertion of four amino acids providing a minimal furin
132 cleavage site (R-R-A-R₆₈₅↓) in contrast to the S protein of SARS-CoV. Instead, similar to
133 SARS-CoV the S2' cleavage site of SARS-CoV-2 S possesses a paired dibasic motif with a
134 single KR segment (KR₈₁₅↓) that is recognized by trypsin-like serine proteases.

135 In the present study we demonstrate that the S protein of SARS-CoV-2 is activated by
136 TMPRSS2 and furin. We also show that inhibitors against both proteases strongly suppress
137 virus replication in human airway epithelial cells and that the combination of both types of
138 inhibitors has a synergistic effect on virus reduction. Our results show that this approach has
139 a high therapeutic potential for treatment of COVID-19.

140

141

142 **Results**

143

144 *Cleavage of SARS-CoV-2 S1/S2 site FRET-substrates by furin*

145 The S1/S2 cleavage site of the novel emerged SARS-CoV-2 has been shown to possess a
146 minimal furin consensus motif of the sequence R-R-A-R↓ with an alanine instead of a basic
147 residue in P2 position (Fig. 1B; Coutard et al., 2020; Walls et al., 2020). Only few furin
148 substrates possess a nonbasic residue in P2 position, such as *Pseudomonas aeruginosa*
149 exotoxin A or Shiga toxin (Rockwell et al., 2002; Garten, 2018). To test, whether the S1/S2
150 sequence of SARS-CoV-2 S protein is efficiently cleaved by furin, a small series of
151 Fluorescence Resonance Energy Transfer (FRET) substrates was synthesized (Fig. 2A). All
152 compounds possess a 3-nitrotyrosine amide as P4' residue and a 2-amino-benzoyl
153 fluorophore in P7 position. The analogous sequences of the S proteins from MERS-CoV,
154 SARS-CoV, and avian infectious bronchitis virus (IBV) strain Beaudette were prepared as
155 reference substrates. Moreover, two FRET substrates of the SARS-CoV-2 S1/S2 cleavage
156 site with P2 A→K and A→R mutations were synthesized, to evaluate whether they could
157 constitute even more efficient cleavage sites for furin than the wild-type. The FRET
158 substrates were tested in an enzyme kinetic assay with human furin, and their cleavage
159 efficiency is shown in Figure 2B. The FRET substrate of the SARS-CoV-2 S1/S2 cleavage
160 site was efficiently cleaved by recombinant furin. In contrast, the monobasic SARS-CoV
161 FRET substrate was not processed by furin. The MERS-CoV S1/S2 FRET substrate
162 possessing a dibasic R-X-X-R motif was cleaved by furin approximately 10-fold less
163 efficiently than the best substrates of this FRET series. The FRET substrate SARS-CoV-

164 2_M1, which contains an optimized furin recognition site by virtue of an A→K mutation in P2
165 position, was cleaved with similar efficiency compared to the wild-type sequence. However,
166 substitution of A→R in the P2 position strongly enhanced cleavage by furin. As expected, the
167 analogous reference sequence of IBV was also processed by furin very efficiently. The data
168 show that the R-R-A-R motif at the S1/S2 cleavage site of SARS-CoV-2 S is efficiently
169 cleaved by furin *in vitro*.

170

171 **SARS-CoV-2 spike protein is cleaved by both furin and TMPRSS2**

172 We next examined whether the SARS-CoV-2 S protein is cleaved by endogenous furin in
173 HEK293 cells. Cells were transiently transfected with pCAGGS plasmid encoding the SARS-
174 CoV-2 S protein with a C-terminal Myc-6xHis-tag, and incubated in the absence and
175 presence of the potent synthetic furin inhibitor MI-1851 (cf. Fig. S1; manuscript in
176 preparation). At 24 h post transfection, cell lysates were subjected to SDS-PAGE and
177 Western blot analysis using antibodies against the Myc epitope. As shown in Fig. 2C, the
178 uncleaved precursor S and the S2 subunit were detected in the absence of MI-1851,
179 indicating that S is cleaved by endogenous proteases at the S1/S2 site in HEK293 cells. S
180 cleavage was efficiently prevented by MI-1851. In contrast, S cleavage was not prevented by
181 the trypsin-like serine protease inhibitor aprotinin. Thus, the data indicate that SARS-CoV-2
182 S protein is cleaved by furin at the S1/S2 site in HEK293 cells.

183 We then investigated SARS-CoV-2 S cleavage by TMPRSS2. Since HEK293 cells do not
184 express endogenous TMPRSS2 (unpublished data; see also www.proteinatlas.org), we co-
185 transfected the cells with pCAGGS-S-Myc-6xHis and pCAGGS-TMPRSS2. Then, the cells
186 were incubated in the absence or presence of MI-1851 to suppress S cleavage by
187 endogenous furin. Interestingly, two S cleavage products of approximately 95 and 80 kDa,
188 respectively, were detected upon co-expression of TMPRSS2 in the absence of MI-1851
189 (Fig. 2C), most likely S2 and S2', as they can both be detected by the Myc-specific antibody
190 (cf. Fig. 1A). In the presence of MI-1851, only a minor S2 protein band was detected.
191 However, the amount of S2' protein present in transient TMPRSS2 expressing cells was
192 similar in MI-1851 treated and untreated cells, suggesting that S cleavage at the S2' site is
193 only caused by TMPRSS2 activity. The small amount of S2 protein detected in TMPRSS2-
194 expressing cells in the presence of MI-1851 was likely due to residual furin activity rather
195 than cleavage of S at the S1/S2 site by TMPRSS2. Together, the data show that SARS-CoV-
196 2 can be cleaved by furin and by TMPRSS2. The data further suggest that the proteases
197 cleave S at different sites with furin processing the S1/S2 site and TMPRSS2 cleaving at the
198 S2' site.

199

200 *Knockdown of TMPRSS2 prevents proteolytic activation and multiplication of SARS-CoV-2 in*
201 *Calu-3 human airway epithelial cells*

202 Next, we wished to investigate whether TMPRSS2 is involved in proteolytic activation and
203 multicycle replication of SARS-CoV-2 in Calu-3 human airway epithelial cells. To specifically
204 knockdown TMPRSS2 activity, we previously developed an antisense peptide-conjugated
205 phosphorodiamidate morpholino oligomer (PPMO) (Böttcher-Friebertshäuser et al., 2011).
206 PPMO are single-stranded nucleic acid-like compounds, composed of a morpholino oligomer
207 covalently conjugated to a cell-penetrating peptide, and can interfere with gene expression
208 by sterically blocking complementary RNAs. PPMO are water-soluble and achieve entry into
209 cells and tissues without assisted delivery (reviewed in Stein, 2008; Moulton and Moulton,
210 2010). The previously developed PPMO T-ex5 interferes with correct splicing of TMPRSS2
211 pre-mRNA, resulting in the production of mature mRNA lacking exon 5 and consequently
212 expression of a truncated TMPRSS2 form that is enzymatically inactive. Using T-ex5 PPMO-
213 mediated knockdown of TMPRSS2 activity, we were able to identify TMPRSS2 as the major
214 influenza A virus activating protease in Calu-3 cells and primary human airway epithelial cells
215 and of influenza B virus in primary human type II pneumocytes (Böttcher-Friebertshäuser et
216 al., 2011; Limburg et al., 2019).

217 Here, Calu-3 cells were treated once with T-ex5 PPMO for 24 h prior to infection with SARS-
218 CoV-2 in order to inhibit the production of normal TMPRSS2-mRNA and deplete
219 enzymatically active TMPRSS2 present in the cells. The cells were then inoculated with
220 SARS-CoV-2 at a low multiplicity of infection (MOI) of 0.001, further incubated without
221 additional PPMO treatment for 72 h, then fixed and immunostained using an antiserum
222 against the 2002 SARS-CoV. As shown in Fig. 3A, a strong cytopathic effect (CPE) and
223 efficient spread of SARS-CoV-2 infection was visible in Calu-3 cells treated with a negative-
224 control PPMO of nonsense sequence designated as “scramble” as well as untreated cells
225 that were used as controls. In contrast, no CPE and only small foci of infection were
226 observed in T-ex5 PPMO treated cells at 72 h p.i. (Fig. 3A). To examine SARS-CoV-2
227 activation and multicycle replication in PPMO treated cells in more detail, Calu-3 cells were
228 treated with PPMO for 24 h prior to infection, then inoculated with virus at a MOI of 0.001 for
229 1.5 h and incubated for 72 h in the absence of further PPMO, as described above. At
230 different time points virus titers in supernatants were determined by tissue culture infection
231 dose 50 % (TCID₅₀) end-point dilution. T-ex5 PPMO treatment dramatically reduced virus
232 titers in Calu-3 cells, by 1,000- and 4,000-fold at 16 and 24 h p.i., respectively, and 180-fold
233 at 48 h p.i. (Fig. 3B).

234 To confirm knockdown of enzymatically active TMPRSS2 expression, Calu-3 cells were
235 treated with PPMO or remained untreated for 24 h, after which TMPRSS2-specific mRNA
236 was isolated and analysed by RT-PCR as described previously (Böttcher-Friebertshäuser et
237 al., 2011). Total RNA was analysed with primers designed to amplify nucleotides 108 to 1336
238 of TMPRSS2-mRNA. A full-length PCR product of 1228 bp was amplified from untreated and
239 scramble PPMO treated Calu-3 cells, whereas a shorter PCR fragment of about 1100 bp was
240 amplified from T-ex5 PPMO-treated cells (Fig. 3C). Sequencing revealed that the truncated
241 TMPRSS2-mRNA lacked the entire exon 5 (data not shown). To further confirm that T-ex5
242 PPMO single dose treatment prior to infection still interferes with TMPRSS2-mRNA splicing
243 at 72 h p.i., total RNA was isolated from infected cells at 72 h p.i. and amplified as described
244 above. As shown in Fig. 3C, the majority of TMPRSS2-mRNA amplified from T-ex5 treated
245 cells at 72 h p.i. lacked exon 5. The data demonstrate that T-ex5 was very effective at
246 producing exon skipping in TMPRSS2-pre-mRNA and, thus, at inhibiting expression of
247 enzymatically active protease, during the virus growth period in Calu-3 cells. However, a
248 small band of the full-length PCR product was visible after 72 h p.i., indicating low levels of
249 expression of enzymatically active TMPRSS2 at later time points of the virus growth period,
250 which may explain the increase in virus titers observed at 48 h p.i. (cf. Fig. 3B). Cell viability
251 was not affected by T-ex5 PPMO treatment of Calu-3 cells, as shown in Fig. 3D and
252 described previously (Böttcher-Friebertshäuser et al., 2011; Limburg et al., 2019).
253 Together, our data identify TMPRSS2 as host cell factor essential for SARS-CoV-2 activation
254 and multiplication in Calu-3 cells and show that downregulation of TMPRSS2 activity
255 dramatically blocks SARS-CoV-2 replication.

256

257 *Inhibition of either TMPRSS2 or furin activity suppresses multicycle replication of SARS-
258 CoV-2 in human airway epithelial cells*

259 We next investigated the efficacy of different inhibitors of trypsin-like serine proteases, also
260 inhibiting TMPRSS2, on preventing SARS-CoV-2 activation by TMPRSS2 in Calu-3 cells. We
261 used the natural broad range serine protease inhibitor aprotinin from bovine lung and two
262 prospective peptide mimetic inhibitors of TMPRSS2, MI-432 (Hammami et al., 2012) und MI-
263 1900 (Fig. S1). Aprotinin has long been known to prevent proteolytic activation and
264 multiplication of influenza A virus in cell cultures and mice. Furthermore, inhalation of
265 aerosolized aprotinin by influenza patients markedly reduced the duration of symptoms
266 without causing side effects (Zhirnov et al., 2011). MI-432 was shown to efficiently inhibit
267 proteolytic activation and multiplication of influenza A virus in Calu-3 cells (Meyer et al.,
268 2013). The inhibitor MI-1900 is a monobasic and structurally related analog of the dibasic
269 inhibitor MI-432.

270 To examine the antiviral efficacy of the protease inhibitors against SARS-CoV-2, Calu-3 cells
271 were infected with the virus at a low MOI of 0.001 for 1.5 h, after which the inoculum was
272 removed and the cells incubated in the presence of the inhibitors at the indicated
273 concentrations for 72 h. The cells were fixed and immunostained using a rabbit antiserum
274 originally produced against SARS-CoV. As shown in Fig. 4, strong CPE and efficient spread
275 of SARS-CoV-2 infection was visible in Calu-3 cells in the absence of protease inhibitors.
276 Spread of SARS-CoV-2 infection and virus induced CPE was efficiently inhibited by aprotinin
277 treatment in a dose-dependent manner and only a few infected cells were visible in Calu-3
278 cultures treated with 20-50 μ M aprotinin. Even at lower concentration of 10 μ M the spread of
279 SARS-CoV-2 was greatly reduced and CPE markedly prevented. Treatment with peptide
280 mimetic TMPRSS2 inhibitors MI-432 and MI-1900 also strongly prevented SARS-CoV-2
281 multiplication and CPE in Calu-3 cells in a dose-dependent manner, although less potently
282 than aprotinin. At 20-50 μ M of MI-432 or MI-1900 only small foci of infection were visible. At a
283 concentration of 10 μ M, virus spread and CPE in MI-432 treated cells were still markedly
284 reduced compared to control cells, whereas CPE and spread of infection was observed in
285 the presence of 10 μ M MI-1900, although still reduced compared to control cells. The data
286 demonstrate that SARS-CoV-2 multiplication in Calu-3 human airway cells can be strongly
287 suppressed by aprotinin and the synthetic TMPRSS2 inhibitors MI-432 and MI-1900.

288 The observed efficient cleavage of transient expressed SARS-CoV-2 S protein by furin in
289 HEK293 cells prompted us to investigate if furin is involved in SARS-CoV-2 activation in
290 Calu-3 cells. Therefore, virus spread in Calu-3 cells was analysed in the presence of the furin
291 inhibitor MI-1851. Interestingly, MI-1851 strongly inhibited SARS-CoV-2 spread at even the
292 lowest concentration of 10 μ M, indicating that furin is critical for SARS-CoV-2 activation and
293 multiplication in these cells (Fig. 4). Finally, to examine whether endosomal cathepsins are
294 involved in SARS-CoV-2 activation in Calu-3 cells, multicycle virus replication was
295 determined in the presence of the cathepsin inhibitor E64d. Cathepsin L was shown to
296 cleave the S protein of 2002 SARS-CoV S close to the S1/S2 site (R667) at T678 *in vitro*
297 (Bosch et al., 2008). Here, strong CPE and foci of infection were observed in E64d-treated
298 cells even at the highest dose of 50 μ M, similar to that observed in DMSO-treated as well as
299 untreated control cells, indicating that SARS-CoV-2 activation in Calu-3 cells is independent
300 of endosomal cathepsins.

301 In sum, our data demonstrate that inhibition of either TMPRSS2 or furin strongly inhibits
302 SARS-CoV-2 in Calu-3 human airway cells, indicating that both proteases are critical for S
303 activation. In contrast, endosomal cathepsins are dispensable or not involved at all in SARS-
304 CoV-2 activation in these cells.

305

306 *Growth kinetics of SARS-CoV-2 in protease inhibitor-treated Calu-3 cells*

307 To analyse inhibition of SARS-CoV-2 activation and multiplication by the different protease
308 inhibitors in more detail, we performed virus growth kinetics in inhibitor treated cells. Calu-3
309 cells were inoculated with SARS-CoV-2 at a MOI of 0.001 and then incubated in the
310 presence of 10 or 50 μ M of the different protease inhibitors. At 16, 24, 48 and 72 h p.i. the
311 viral titer in supernatants was determined by TCID₅₀ titration. Untreated cells and cells
312 treated with DMSO alone were used as controls. SARS-CoV-2 replicated to high titers within
313 24-48 h in untreated and DMSO treated cells Calu-3 cells (Fig. 5A). Aprotinin suppressed
314 virus replication 20- to 35-fold compared to control cells even at a concentration of 10 μ M.
315 The TMPRSS2 inhibitor MI-432 reduced virus titers in a dose-dependent manner with 5-fold
316 reduction in virus titers at a concentration of 10 μ M and 14-fold at 50 μ M. Treatment of cells
317 with TMPRSS2 inhibitor MI-1900 reduced virus titers in a manner similar to that of MI-432 at
318 10 μ M. However, treatment with 50 μ M MI-1900 caused strong inhibition of SARS-CoV-2
319 replication with 25- to 70-fold reduced viral titers compared to control cells. The furin inhibitor
320 MI-1851 efficiently suppressed SARS-CoV-2 multiplication in Calu-3 cells, producing a 30- to
321 75-fold reduction in virus titers at a dose of 10 μ M. In contrast, virus multiplication was not
322 affected by treatment with the cathepsin inhibitor E64d, which is in congruence with the data
323 shown in Fig. 4. To provide evidence that inhibition of SARS-CoV-2 replication in inhibitor
324 treated cells was not caused by cytotoxic effects, we analysed cell viability in Calu-3 cells
325 treated with 50 μ M of the different inhibitors for 72 h. As shown in Fig. 5B, evaluation of cell
326 viability revealed no significant cytotoxicity by any of the inhibitors under conditions used in
327 the virus growth experiments.

328 The data demonstrate that SARS-CoV-2 replication can be efficiently reduced by inhibiting
329 either TMPRSS2 or furin activity, demonstrating that both proteases are crucial for SARS-
330 CoV-2 activation.

331

332 *Treatment of SARS-CoV-2 infected Calu-3 cells with a combination of TMPRSS2 and furin
333 inhibitors*

334 Finally, we wished to examine whether the combination of inhibitors against TMPRSS2 and
335 furin shows a synergistic antiviral effect. Therefore, Calu-3 cells were infected with virus as
336 described above and incubated in the presence of aprotinin, MI-432 or MI-1900 in
337 combination with MI-1851 at 10 and 50 μ M each, respectively, for 72 h. Virus titers in
338 supernatants were determined at indicated time points. Single dose treatment of each
339 inhibitor and untreated cells were used as controls. As shown in Fig. 5C, the combination of
340 10 μ M of MI-1851 with either aprotinin or MI-432 showed enhanced antiviral activity against

341 SARS-CoV-2 and 10- to 30-fold reduced virus titers compared to 10 μ M of each inhibitor
342 alone and even caused a 4- to 8-fold reduction in virus titer compared to 50 μ M single
343 inhibitor treatment. Combination of 50 μ M of MI-432 and MI-1851 reduced virus titers 10- to
344 32-fold compared to 50 μ M of each inhibitor alone and thereby dramatically suppressed
345 SARS-CoV-2 multiplication 100- to 250-fold compared to untreated or DMSO treated cells. In
346 contrast, treatment of Calu-3 cells with 50 μ M of MI-1851 and aprotinin did not cause further
347 suppression of virus titers compared to the combination of 10 μ M of each inhibitor. The
348 combination of 10 μ M MI-1851 and MI-1900 did not show enhanced antiviral activity
349 compared to single inhibitor treatments at 10 μ M. However, treatment of cells with 50 μ M of
350 MI-1900 and MI-1851 caused 5-fold reduction in viral titers when compared to cells treated
351 with 50 μ M of each inhibitor alone and thereby dramatically reduced SARS-CoV-2
352 multiplication in Calu-3 cells compared to control cells. We furthermore examined the
353 antiviral activity of a combination of T-ex5 PPMO and furin inhibitor MI-1851 against SARS-
354 CoV-2 in Calu-3 cells. As shown in Fig. 5D, combined treatment of Calu-3 cells with 25 μ M T-
355 ex5 PPMO and 50 μ M MI-1851 almost completely blocked SARS-CoV-2 replication with a
356 nearly 40,000-fold reduction in virus titers at 24 h p.i., and reduced virus titers 1,000-fold at
357 48 h p.i. compared to control cells. Combination of T-ex5 and MI-1851 was synergistic and
358 caused 30- to 10-fold lower virus titers at 16 and 24 h p.i. when compared with single
359 inhibitor treated cells. The data demonstrate that efficient inhibition of S cleavage by a
360 combination of TMPRSS2 and furin inhibitors can block SARS-CoV-2 replication in human
361 airway epithelial cells. Further, our data show that combination of TMPRSS2 and furin
362 inhibitors acts synergistically and allows inhibition of SARS-CoV-2 activation and
363 multiplication at lower doses compared to single protease inhibitor treatment.

364 In conclusion, our data demonstrate that both TMPRSS2 and furin cleave the SARS-CoV-2 S
365 protein and are essential for virus multicycle replication in Calu-3 human airway cells. The
366 results indicate that TMPRSS2 and furin cleave S at different sites - furin at the S1/S2 site
367 and TMPRSS2 at the S2' site - and that TMPRSS2 and furin cannot compensate for each
368 other in SARS-CoV-2 S activation. Hence, inhibition of either one of these critical proteases
369 can render the S protein of SARS-CoV-2 unable to efficiently mediate virus entry and
370 membrane fusion. Therefore, TMPRSS2 and furin provide promising drug targets for
371 treatment of COVID-19, and inhibitors MI-432, MI-1900, MI-1851 as well as T-ex5 PPMO
372 may provide the basis for development of novel protease inhibitors. Our data further
373 demonstrate that aprotinin efficiently prevents proteolytic activation and multiplication of
374 SARS-CoV-2 in human airway cells and is therefore worthy of consideration for further
375 testing and possible development as a therapeutic treatment for COVID-19.

376

377 **Discussion**

378 Proteolytic processing of CoV S is a complex process that requires cleavage at two different
379 sites and is yet not fully understood. The amino acid sequence at the S1/S2 and S2'
380 cleavage sites varies among CoVs (Fig. 1B), suggesting that partially different proteases
381 may be involved in activation. Sequence analyses of the S protein of the novel emerged
382 SARS-CoV-2 suggested that the R-R-A-R motif at the S1/S2 site may be sensitive to
383 cleavage by furin, while the S2' site contains a single R residue that can be cleaved by
384 trypsin-like serine proteases such as TMPRSS2 (Coutard et al., 2020; Walls et al., 2020;
385 Hoffmann et al., 2020). In the present study, we demonstrate that the SARS-CoV-2 S protein
386 is cleaved by furin and by TMPRSS2. Furthermore, we show that multicycle replication of
387 SARS-CoV-2 in Calu-3 human airway cells is strongly suppressed by inhibiting TMPRSS2
388 and furin activity, demonstrating that both proteases are crucial for S activation in these cells.
389 Our data indicate that furin cleaves at the S1/S2 site, whereas TMPRSS2 cleaves at the S2'
390 site. The effective processing of the S1/S2 site by furin was additionally confirmed by
391 comparing the cleavage rates of various FRET substrates derived from the P6-P3' segments
392 of SARS-CoV-2 and other CoVs. The data clearly revealed that due to the 4-mer PRRA
393 insertion a well suited furin cleavage site exists in S of SARS-CoV-2, which is similarly
394 cleaved as the sequence from the IBV CoV, whereas the analogous substrate of SARS-CoV
395 is not processed by furin. Strong inhibition of SARS-CoV-2 replication in Calu-3 cells by
396 synthetic furin inhibitor MI-1851 furthermore suggests that TMPRSS2 does not compensate
397 for furin cleavage at the S1/S2 site. Likewise, strong inhibition of SARS-CoV-2 replication by
398 knockdown of TMPRSS2 activity using T-ex5 PPMO or treatment of Calu-3 cells with
399 aprotinin, MI-432 and MI-1900, respectively, indicates that furin cannot compensate for the
400 lack of TMPRSS2 in S activation. This was further confirmed by using an analogous FRET
401 substrate derived from the S2' cleavage site of the SARS-CoV-2 S protein (Fig. S2). Kinetic
402 measurements clearly revealed that this substrate cannot be cleaved by furin (Fig. S2). Thus,
403 we could experimentally demonstrate for the first time that furin only activates the S1/S2 site,
404 as expected from the amino acid sequence at the cleavage sites (Coutard et al., 2020; Walls
405 et al., 2020). Together, our data indicate that furin and TMPRSS2 cleave S at different sites,
406 and, cleavage by both proteases is crucial to render the S protein active for mediating virus
407 entry and membrane fusion (Fig. 6). Iwata-Yoshikawa et al. showed that TMPRSS2-deficient
408 mice do not suffer from pathology when infected with SARS-CoV and MERS-CoV (Iwata-
409 Yoshikawa et al., 2019). The data demonstrated that TMPRSS2 is essential for multicycle
410 replication and spread of these CoVs similar to what we and others have been observed for
411 certain influenza A virus strains (Hatesuer et al., 2013; Tarnow et al., 2014; Sakai et al.,
412 2014). However, it remains to be determined whether knockout of TMPRSS2 prevents
413 cleavage of the S proteins of SARS-CoV and MERS-CoV at both sites, S1/S2 and S2', or

414 whether another protease is involved in S cleavage similar to what we have observed here
415 for SARS-CoV-2.

416 In cell culture, CoVs can enter cells via two distinct routes: the late endosome where S is
417 cleaved by cathepsins or via the cell-surface or early endosome utilizing trypsin-like
418 proteases for S cleavage (Simmons et al., 2005; Bosch et al., 2008; reviewed in Millet and
419 Whittaker, 2015). However, several recent studies revealed that clinical isolates of human
420 CoV (HCoV) achieve activation by trypsin-like serine proteases and utilize endosomal
421 cathepsins only in the absence of suitable trypsin-like proteases in cell culture (Shirato et al.,
422 2016, 2018). Thus, activation by cathepsins appears to be a mechanism that is acquired by
423 the virus during multiple passaging in cell cultures (Shirato et al., 2018). Congruently, Zhou
424 et al. showed that SARS-CoV pathogenesis in mice was strongly prevented by camostat, a
425 broad-range inhibitor of trypsin-like serine proteases, but not by inhibitors of endosomal
426 cathepsins (Zhuo et al., 2015). Here, we show that the cysteine protease inhibitor E64d that
427 also inhibits cathepsin L and B did not affect SARS-CoV-2 replication in Calu-3 cells,
428 indicating that endosomal cathepsins are dispensable or not involved at all in SARS-CoV-2
429 activation in human airway cells.

430 The presence of a multibasic cleavage site that is processed by ubiquitously expressed furin
431 and, therefore, supports systemic spread of infection, has long been known to be a major
432 determinant of the pathogenicity of HPAIV in poultry (reviewed in Garten and Klenk, 2008). In
433 contrast, the HA of LPAIV is activated at a monobasic cleavage site by trypsin-like serine
434 proteases present in a limited number of tissues limiting spread of infection to these tissues.
435 The S protein of IBV strain Beaudette contains multibasic motifs at the S1/S2 and S2' site
436 (Fig. 1B). IBV belongs to the genus *Gammacoronavirus* and causes a highly contagious,
437 acute respiratory disease of chickens. Cleavage of IBV S protein by furin at the S2' site has
438 been associated with neurotropism in chicken (Cheng et al., 2019). Congruently, here, FRET
439 substrates of the S1/S2 and S2' site of the IBV Beaudette S protein were efficiently cleaved
440 by furin (Fig. 2B and Fig. S2B). However, the advantage of furin-cleavable multibasic motifs
441 at the S1/S2 and/or S2' site for multicycle replication, cellular tropism and pathogenicity of
442 HCoVs remains to be determined. HCoV-OC43 and HCoV-HKU1 possess a furin cleavage
443 motif at the S1/S2 site. In contrast, the S proteins of the 2002 SARS-CoV, HCoV-229E and
444 HCoV-NL63 possess single arginine residues at both cleavage sites (see also Fig. 2B and
445 S2A). Interestingly, among the S proteins of the seven CoV infecting humans only SARS-
446 CoV S lacks the 4-mer insertion at the S1/S2 site (Fig. 1B; Walls et al., 2020). The S protein
447 of MERS-CoV contains a dibasic motif of the sequence R-X-X-R at both S1/S2 and S2' site.
448 It is still controversial whether MERS-CoV is activated by furin in human airway epithelial
449 cells, as its clear role remains to be demonstrated (Gierer et al., 2015; Millet and Whittaker,

450 2014; Burkhard et al., 2014; Matsuyama et al., 2018). Probably, other proteases like the
451 serine protease matriptase/ST14, which also prefers sequences with arginine in P1 and P4
452 position, might be involved. Matriptase is expressed in a broad range of cells and tissues and
453 has been shown to activate the HA of H9N2 influenza A viruses possessing the cleavage site
454 motif R-S-S-R (Baron et al., 2013; reviewed in Böttcher-Friebertshäuser, 2018). Interestingly,
455 a study by Park et al. indicated that cleavage of MERS-CoV S by furin or other PCs at the
456 S1/S2 site takes place in virus-producing cells prior to virus release and can impact the
457 cellular localization of membrane fusion and virus entry into a new cell (Park et al., 2016).
458 Cleavage of MERS-CoV at the S1/S2 site was postulated as a prerequisite for subsequent
459 cleavage of S at the S2' site by host proteases present at the surface or in early endosomes
460 of human airway cells facilitating virus entry independent of S cleavage by cathepsins in the
461 late endosome. However, other HCoV including the 2002 SARS-CoV are described to be
462 released with non-cleaved S from the infected cell. Hence, S cleavage at both sites, S1/S2
463 and S2', has to take place at the stage of entry for these viruses.

464 The present study demonstrates that TMPRSS2 and furin are promising drug targets for the
465 treatment of COVID-19 either by targeting one of these proteases alone or by a combination
466 of furin and TMPRSS2 inhibitors. The used TMPRSS2 inhibitors MI-432 and MI-1900 as well
467 as the furin inhibitor MI-1851 provide promising compounds for further drug development. In
468 search for suitable antiviral therapies against SARS-CoV-2 infections, protease inhibitors that
469 have been approved for other applications may be promising for drug repurposing to treat
470 COVID-19. Aprotinin is a broad range serine protease inhibitor isolated from bovine lung,
471 which is used as a fibrinolysis inhibitor to reduce perioperative bleeding (reviewed in
472 Steinmetzer et al., 2020) and has long been known to inhibit influenza A virus activation and
473 replication in cell culture and in mice *in vivo* (Zhirnov et al., 2011). In a clinical trial, inhalation
474 of aerosolized aprotinin in patients with influenza and parainfluenza markedly reduced the
475 duration of symptoms without causing side effects (Zhirnov et al., 2011). Thus, aprotinin is an
476 inhibitor of TMPRSS2 worthy of consideration for further testing and possible development
477 as a therapeutic treatment for COVID-19. Another promising TMPRSS2 inhibitor candidate
478 for COVID-19 treatment is the broad range protease inhibitor camostat. Camostat mesylate
479 is a phenyl-4-guanidinobenzoate derivative originally developed under the name FOY-305 for
480 the treatment of pancreatitis (Tanaka et al., 1979; Midgley et al., 1994) and has been shown
481 to efficiently inhibit replication of different CoV in cell culture and experimentally infected mice
482 (Kawase et al., 2012; Shirato et al., 2013; Zhou et al., 2015). Recently, Hoffmann et al.
483 showed that pretreatment of human Caco-2 colon cells and human airway cells with
484 camostat mesylate markedly reduced entry of SARS-CoV-2 as well as VSV pseudotypes
485 containing the SARS-CoV-2 S protein (Hoffmann et al., 2020).

486 However, it should be noted that all of these compounds inhibit numerous trypsin-like serine
487 proteases and thus may cause various adverse effects. A specific inhibition of TMPRSS2
488 activity during an acute SARS-CoV-2 infection would provide the most promising approach to
489 reduce side effects by inhibiting virus activation by host cell proteases. TMPRSS2-deficient
490 mice show no discernible phenotype, indicating functional redundancy or compensation of
491 physiological functions by other protease(s) in the host (Kim et al., 2006). Unfortunately,
492 there is no crystal structure of TMPRSS2 available so far, which prohibits a rational structure-
493 based design of more efficient inhibitors of this protease. However, first homology models
494 have been established, which may help for the development of improved TMPRSS2
495 inhibitors in the future (Steinmetzer and Hardes, 2018; Rensi et al. <https://chemrxiv.org>).

496 PPMO are highly selective inhibitors of target gene expression. They bind to a
497 complementary sequence in target mRNA and can affect gene expression by steric blockage
498 of translation initiation or pre-mRNA splicing. The demonstration of T-ex5 PPMO efficacy in
499 the present study suggests that reducing TMPRSS2 expression by use of a mRNA-directed
500 approach in general and by PPMO in particular is worthy of further consideration.
501 Importantly, in various experimental animal models of other viral infections and disease,
502 PPMO were able to be transported to lung tissue after intranasal administration and
503 produced strong reductions in virus growth and virus-induced pathology (Gabriel et al., 2008;
504 Lupfer et al., 2008; Lai et al., 2008; Opriessnig et al., 2011).

505 Very effective furin inhibitors containing a C-terminal 4-amidinobenzylamide residue have
506 been developed in recent years. Several of these analogues have been successfully used to
507 inhibit the replication of numerous furin dependent human pathogenic viruses like H5N1
508 influenza A virus, Chikungunya virus, West-Nile virus and Dengue-2 virus, Mumps virus or
509 respiratory syncytial virus (RSV) (reviewed in Steinmetzer and Hardes, 2018; Krüger et al.,
510 2018; Van Lam van et al., 2019). So far, these inhibitors have only been used in virus
511 infected cell cultures, but not in animal models. However, the less potent furin inhibitor hexa-
512 D-arginine has been used in mice and rats to protect them against *Pseudomonas aeruginosa*
513 Exotoxin A and anthrax toxemia (Sarac et al., 2002, 2004). Therefore, it can be speculated
514 that a specific furin inhibition in the respiratory tract and lung by inhalative treatment of e.g.
515 MI-1851 or structurally related compounds could be possible without severe side reactions,
516 despite many physiological functions of furin.

517 Here, the combination of the TMPRSS2 inhibitors aprotinin or MI-432 with furin inhibitor MI-
518 1851 showed enhanced antiviral activity against SARS-CoV-2 in human airway cells and
519 supported strong reduction of virus multiplication at lower doses compared to treatment with
520 each inhibitor alone. Therefore, the combination of TMPRSS2 and furin inhibitors provides a
521 promising therapeutic strategy for treatment of SARS-CoV-2 infections that not only may

522 enhance antiviral effects, but may also reduce drug toxicity and undesirable side effects by
523 allowing reductions of the inhibitor doses. Notably, inhibition of TMPRSS2 and furin acts on
524 the same target and our data show that inhibition of S cleavage at one of the two sites is
525 sufficient to suppress SARS-CoV-2 replication by reduced production of infectious progeny
526 virus containing inactive S. Thus, the combination of TMPRSS2 and furin inhibitors can act
527 synergistically until S cleavage at one or two sites is completely prevented. The combination
528 of protease inhibitors with antiviral compounds provides an approach that may show even
529 more synergistic antiviral activity at lower drug doses and may furthermore exclude the
530 development of drug resistant viruses. The combination of TMPRSS2 and furin inhibitors,
531 respectively, with the neuraminidase inhibitor oseltamivir carboxylate has been shown to
532 block influenza A virus replication in human airway cells at remarkably lower concentration of
533 each inhibitor as compared to single inhibitor treatment (Böttcher-Friebertshäuser et al.,
534 2012). Combination of a furin inhibitor with oseltamivir carboxylate and the antiviral
535 compounds ribavirin and favipiravir, respectively, efficiently blocked multicycle replication of
536 HPAIV of subtype H5N1 and H7N1 in cell cultures (Lu et al., 2015; Garten et al., 2015).
537 Thus, combination of protease inhibitors (e.g. aprotinin or camostat) and antivirals provides a
538 promising approach to block SARS-CoV-2 replication that should be tested in cell cultures
539 and animal models and should furthermore be considered as therapeutic strategy for the
540 treatment of COVID-19.

541 In summary, we demonstrate that TMPRSS2 and furin are essential for activation and
542 multiplication of the novel emerged SARS-CoV-2 in human airway epithelial cells and provide
543 promising drug targets for treatment of COVID-19. TMPRSS2 and furin have been shown to
544 be involved in the proteolytic activation of a broad range of viruses. However, the
545 development of host protease inhibitors as a preventative and/or therapeutic strategy for the
546 treatment of virus infections has been minimal to date. Our data demonstrate the high
547 potential of protease inhibitors as drugs for SARS-CoV-2 treatment and highlight the urgent
548 need of drug development and repurposing of potent host protease inhibitors for the
549 treatment of virus infections in general and emerging CoV infections in particular.

550

551 **Acknowledgement**

552 We are grateful to Christian Drosten for providing the virus. We thank Iris Lindberg for
553 providing recombinant furin. This work was funded by the LOEWE Center DRUID (project
554 D1), by the German Center for Infection Research (DZIF), and by the Deutsche
555 Forschungsgemeinschaft (DFG, German Research Foundation) SFB 1021 (project B07). We
556 thank Diana Kruhl for excellent technical assistance.

557

558 **Materials and Methods**

559

560 **Cells.** Calu-3 human airway epithelial cells (ATCC® HTB55) were cultured in Dulbecco's
561 modified Eagle's medium (DMEM)-Ham F-12 medium (1:1) (Gibco) supplemented with 10%
562 fetal calf serum (FCS), penicillin, streptomycin, and glutamine, with fresh culture medium
563 replenished every 2 to 3 days. Vero E6 (ATCC® CRL-1586) and HEK293 (ATCC® CRL-
564 1573) cells were maintained in DMEM supplemented with 10 % FCS, antibiotics and
565 glutamine.

566

567 **Virus and plasmids.** Experiments with SARS-CoV-2 were performed under biosafety level 3
568 (BSL-3) conditions. The virus used in this study was SARS-CoV-2 isolate Munich 929 (kindly
569 provided by Christian Drosten, Institute of Virology, Charité Universitätsmedizin Berlin,
570 Germany). Virus stock was propagated on Vero E6 cells in DMEM medium with 1 % FCS for
571 72 h. Cell supernatant was cleared by low-speed centrifugation and stored at -80°C.
572 The cDNA encoding the SARS-CoV-2 spike protein of isolate Wuhan-Hu-1 (GenBank
573 accession number MN908947; codon-optimized, sequence available upon request) with a C-
574 terminal Myc-6xHis-tag was synthesized at Eurofins and subcloned into the pCAGGS
575 expression plasmid using Xhol and Nhel restriction sites (pCAGGS-S-Myc-6xHis).
576 Expression plasmid pCAGGS-TMPRSS2 encoding the cDNA of human TMPRSS2 has been
577 described previously (Böttcher et al., 2006).

578

579 **Antibodies.** A polyclonal serum against 2002 SARS-CoV was generated by immunization of
580 rabbits with inactivated SARS-CoV. A monoclonal mouse antibody against the C-terminal
581 Myc-tag was purchased from CellSignaling Technology (2276S). A monoclonal mouse anti-
582 beta actin antibody was purchased from Abcam (ab6276). Horseradish peroxidase (HRP)-
583 conjugated secondary antibodies were purchased from DAKO.

584

585 **PPMO.** Phosphorodiamidate morpholino oligomers (PMO) were synthesized at Gene Tools
586 LLC (Corvallis, OR, USA). PMO sequences (5' to 3') were
587 CAGAGTTGGAGCACTTGCTGCCCA for T-ex5 and CCTCTTACCTCAGTTACAATTATA
588 for scramble. The cell-penetrating peptide (RXR)4 (where R is arginine and X is 6-
589 aminohexanoic acid) was covalently conjugated to the 3' end of each PMO through a
590 noncleavable linker, to produce peptide-PMO (PPMO), by methods described previously
591 (Abes et al., 2006).

592

593 **Protease inhibitors.** Aprotinin was purchased from AppliChem, the cysteine protease
594 inhibitor E64d from Sigma-Aldrich (E8640). The synthetic inhibitors of TMPRSS2 and furin
595 were synthesized according to previous methods (Hammami et al., 2012; Hardes et al.,
596 2015). Stock solutions of protease inhibitors were prepared in double distilled water
597 (aprotinin, MI-432, MI-1851) or sterile DMSO (MI-1900, E64d) and stored at -20°C.
598

599 **Synthesis of FRET substrates**

600 The peptides were synthesized by automated solid phase peptide synthesis on a Syro 2000
601 synthesizer (MultiSynTech GmbH, Witten, Germany) using approximately 100 mg Rink-
602 amide-MBHA resin (loading 0.68 mmol/g) for each 2 ml reaction vessel and a standard
603 Fmoc-protocol with double couplings (approximately 4-fold excess of Fmoc amino acid,
604 HOEt and HBTU, respectively, and 8 equiv. DIPEA, 2 × 2 h coupling time) as described
605 recently (Hardes et al., 2013). After final coupling of Boc-2-aminobenzoic acid, the resin was
606 washed with 20 % piperidine in DMF (5 and 15 min) to remove an acylation on the 3-
607 nitrotyrosine (Singh et al., 2002). The peptides were cleaved from the resin and deprotected
608 by a mixture of TFA/triisopropylsilane/water (95/2.5/2.5, v/v/v) over 2 h at room temperature,
609 followed by precipitation in cold diethyl ether. All peptides were purified by preparative
610 reversed-phase HPLC to more than 95 % purity based on the detection at 220 nm, and
611 finally obtained as lyophilized TFA-salts.

612 **Enzyme kinetic measurements with recombinant soluble human furin**

613 The measurements were performed in black 96-well plates (Nunc, Langenselbold) at room
614 temperature with a microplate reader (Safire2, Tecan, Switzerland) at λ_{ex} 320 nm and λ_{em} 405
615 nm. Each well contained 20 μL of the substrate solution (dissolved in water), and 150 μL
616 buffer (100 mM HEPES, 0.2 % Triton X-100, 2 mM CaCl₂, 0.02 % Natriumazid und 1 mg/mL
617 BSA, pH 7.0). The measurements were started by addition of 20 μL furin (Kacprzak et al.,
618 2004) solution (0.5 nM in assay). The measurements were performed for 5 min, and the
619 steady-state rates were calculated from the slopes of the progress curves.
620

621 **RNA isolation, RT-PCR analysis of exon skipping, and RT-qPCR analysis of protease**
622 **transcripts.** For analysis of TMPRSS2-mRNA from PPMO-treated Calu-3 cells, cells were
623 incubated with the indicated concentrations (25 μM) of T-ex5 or scramble PPMO or without
624 PPMO in PPMO medium (DMEM supplemented with 0.1 % BSA, antibiotics, and glutamine)
625 for 24 h. Total RNA was isolated at the indicated time points using the RNeasy Mini kit
626 (QIAGEN) according to the manufacturer's protocol. Reverse transcription-PCR (RT-PCR)
627 was carried out with total RNA using the one-step RT-PCR kit (QIAGEN) according to the
628 supplier's protocol. To analyse-TMPRSS2 mRNAs for exon skipping, primers TMPRSS2-

629 108fwd (5`-CTA CGA GGT GCA TCC-3`) and TMPRSS2-1336rev (5`-CCA GAG GCC CTC
630 CAG CGT CAC CCT GGC AA-3`), designed to amplify a full-length PCR product of 1,228 bp
631 from control cells and a shorter PCR fragment of about 1,100 bp lacking exon 5 from T-ex5-
632 treated cells (Böttcher-Friebertshäuser et al., 2011) were used. RT-PCR products were
633 resolved on a 0.8 % agarose gel stained with ethidium bromide.

634

635 **Infection of cells and multicycle virus replication in the presence of protease inhibitors**
636 **or PPMO.** SARS-CoV-2 infection experiments of Calu-3 cells were performed in serum-free
637 DMEM supplemented with glutamine and antibiotics (DMEM++). For analysis of multicycle
638 replication kinetics Calu-3 cells were seeded in 12-well plates and grown to 90 % confluence.
639 Cells were then inoculated with virus at a multiplicity of infection (MOI) of 0.001 in DMEM++
640 for 1.5 h, washed with PBS, and incubated in DMEM supplemented with 3 % FCS, glutamine
641 and antibiotics (DMEM+++) with or without addition of protease inhibitors or DMSO to the
642 medium for 72 h. At 16, 24, 48, and 72 h postinfection (p.i.), supernatants were collected,
643 and viral titers were determined by tissue culture infection dose 50 % (TCID₅₀) titration as
644 described below. In addition, cells were fixed and immunostained against viral proteins as
645 described below at 72 h p.i. to evaluate virus spread and virus-induced CPE.

646 For PPMO treatment, Calu-3 cells were incubated with 25 μ M T-ex5 or scramble PPMO or
647 remained untreated in PPMO medium for 24 h prior to infection. Cells were infected as
648 described above and incubated in DMEM++ without PPMO for 72 h.

649

650 **Virus titration by TCID₅₀.** Viral supernatants were serial diluted in DMEM++. Each infection
651 time point was titrated in 4 replicates from 5¹ to 5¹¹. Subsequently, 100 μ l of each virus
652 dilution were transferred to Calu-3 cells grown in 96-well plates containing 100 μ l DMEM++
653 and incubated for 72 h. Viral titers were determined with Spearman and Kärber algorithm
654 described in Hierholzer and Killington et al., 1996.

655

656 **Transient expression of SARS CoV-2 S protein in HEK293 cells.** For transient expression
657 of SARS-CoV-2 S protein 60 % confluent HEK293 cells were co-transfected with 1.6 μ g of
658 pCAGGS-S-Myc-6xHis and either 15 ng of empty pCAGGS vector or pCAGGS-TMPRSS2
659 using Lipofectamine® 2000 (Invitrogen) according to the manufacturers protocol for 48 h.
660 Cells were harvested and centrifuged for 5 min at 8.000 x g. Subsequently cells were
661 subjected to SDS-PAGE and Western blot analysis as described below.

662

663 **SDS-PAGE and Western blot analysis.** Cells were washed with PBS, lysed in CellLytic™ M
664 buffer (Sigma Aldrich) with a protease inhibitor cocktail (Sigma Aldrich, P8340), resuspended
665 in reducing SDS-PAGE sample buffer, and heated at 95 °C for 10 min. Proteins were

666 subjected to SDS-PAGE (10 % acrylamid gel), transferred to a polyvinylidene difluoride
667 (PVDF) membrane (GE Healthcare), and detected by incubation with primary antibodies and
668 species-specific peroxidase-conjugated secondary antibodies. Proteins were visualized using
669 the ChemiDoc XRS system with Image Lab software (Bio-Rad).

670

671 **Immunohistochemical staining and microscopy.** To visualize viral spread in SARS-CoV-2
672 infected Calu-3 cells, immunohistochemical staining was performed. Calu-3 cells were fixed
673 72 h post infection in 4 % paraformaldehyde (PFA) for 36 h at 4 °C. The cells were
674 permeabilized with 0.3 % Triton-X-100 (Sigma Aldrich) for 20 min at room temperature (RT).
675 The cells were incubated with a polyclonal rabbit serum against 2002 SARS-CoV for 1.5 h at
676 RT, a species-specific peroxidase-conjugated secondary antibody for 1 h at RT and
677 subsequently stained using the peroxidase substrate KPL TrueBlue™ (Seracare) and further
678 analysed on a Leica Dmi1 microscope.

679

680 **Cell viability assay.** Cell viability was assessed by measuring the cellular ATP content using
681 the CellTiterGlo® luminescent cell viability assay (Promega). Calu-3 cells grown in 96-well
682 plates were incubated with 25 µM of each PPMO or 50 µM of each of the protease inhibitors
683 for 24 and 72 h, respectively. Subsequently, cells were incubated with the substrate
684 according to the manufacturer's protocol. Luminescence was measured using a 96-well plate
685 (Nunc) with a luminometer (Centro LB 960; Berthold Technologies). The absorbance values
686 of PPMO- or inhibitor-treated cells were converted to percentages by comparison to
687 untreated control cells, which were set at 100 % cell viability.

688

689

690 **References**

691
692 Abes S, Moulton HM, Clair P, Prevot P, Youngblood DS, Wu RP, Iversen PL, Lebleu B. 2006.
693 Vectorization of morpholino oligomers by the (R-Ahx-R)4 peptide allows efficient splicing correction in
694 the absence of endosomolytic agents. *J Control Release* 116:304-13.

695 Baron J, Tarnow C, Mayoli-Nüssle D, Schilling E, Meyer D, Hammami M, Schwalm F, Steinmetzer T,
696 Guan Y, Garten W, Klenk HD, Böttcher-Frieberthhäuser E. 2013. Matriptase, HAT, and TMPRSS2
697 activate the hemagglutinin of H9N2 influenza A viruses. *J Virol* 87:1811-20.

698 Belouzard S, Chu VC, Whittaker GR. 2009. Activation of the SARS coronavirus spike protein via
699 sequential proteolytic cleavage at two distinct sites. *Proc Natl Acad Sci U S A* 106:5871-6.

700 Bosch BJ, Bartelink W, Rottier PJ. 2008. Cathepsin L functionally cleaves the severe acute respiratory
701 syndrome coronavirus class I fusion protein upstream of rather than adjacent to the fusion peptide. *J*
702 *Virol* 82:8887-90.

703 Böttcher E, Matrosovich T, Beyerle M, Klenk HD, Garten W, Matrosovich M. 2006. Proteolytic
704 activation of influenza viruses by serine proteases TMPRSS2 and HAT from human airway epithelium.
705 *J Virol* 80:9896-8.

706 Böttcher-Frieberthhäuser E, Lu Y, Meyer D, Sielaff F, Steinmetzer T, Klenk HD, Garten W. 2012.
707 Hemagglutinin activating host cell proteases provide promising drug targets for the treatment of
708 influenza A and B virus infections. *Vaccine* 30:7374-80.

709 Böttcher-Frieberthhäuser E, Stein DA, Klenk HD, Garten W. 2011. Inhibition of influenza virus infection
710 in human airway cell cultures by an antisense peptide-conjugated morpholino oligomer targeting the
711 hemagglutinin-activating protease TMPRSS2. *J Virol* 85:1554-62.

712 Böttcher-Frieberthhäuser E. 2018. Membrane-Anchored Serine Proteases: Host Cell Factors in
713 Proteolytic Activation of Viral Glycoproteins. In: Böttcher-Frieberthhäuser E., Garten W., Klenk H. (eds)
714 Activation of Viruses by Host Proteases. Springer, Cham, p.153-203. Review.

715 Bugge TH, Antalis TM, Wu Q. Type II transmembrane serine proteases. 2009. *J Biol Chem*
716 284:23177-81. Review.

717 Burkard C, Verheije MH, Wicht O, van Kasteren SI, van Kuppeveld FJ, Haagmans BL, Pelkmans L,
718 Rottier PJ, Bosch BJ, de Haan CA. 2014. Coronavirus cell entry occurs through the endo-/lysosomal
719 pathway in a proteolysis-dependent manner. *PLoS Pathog* 10:e1004502.

720 Cheng J, Zhao Y, Xu G, Zhang K, Jia W, Sun Y, Zhao J, Xue J, Hu Y, Zhang G. 2019. The S2 Subunit
721 of QX-type Infectious Bronchitis Coronavirus Spike Protein Is an Essential Determinant of
722 Neurotropism. *Viruses* 11:pii: E972.

723 Coutard B, Valle C, de Lamballerie X, Canard B, Seidah NG, Decroly E. 2020. The spike glycoprotein
724 of the new coronavirus 2019-nCoV contains a furin-like cleavage site absent in CoV of the same
725 clade. *Antiviral Res* 176:104742.

726 Follis KE, York J, Nunberg JH. 2006. Furin cleavage of the SARS coronavirus spike glycoprotein
727 enhances cell-cell fusion but does not affect virion entry. *Virology* 350:358-69.

728 Gabriel G, Nordmann A, Stein DA, Iversen PL, Klenk HD. 2007. Morpholino Oligomers Targeting PB1
729 and NP Genes Enhance Survival of Mice Infected with Highly Pathogenic Influenza A H7N7 Virus.
730 *Journal of General Virology* 89:939-48.

731
732 Garten W, Braden C, Arendt A, Peitsch C, Baron J, Lu Y, Pawletko K, Hardes K, Steinmetzer T,
733 Böttcher-Frieberthhäuser E. 2015. Influenza virus activating host proteases: Identification, localization
734 and inhibitors as potential therapeutics. *Eur J Cell Biol* 94:375-83.

735 Garten W, Klenk HD. 2008. Cleavage activation of the influenza virus hemagglutinin and its role in
736 pathogenesis. In: Klenk HD, Matrosovich MN, Stech J (eds) *Avian Influenza*. Karger, Basel, pp 156-
737 167. Review.

738 Garten, W. 2018. Characterization of Proprotein Convertases and Their Involvement in Virus
739 Propagation. In: Böttcher-Friebertshäuser E., Garten W., Klenk H. (eds) *Activation of Viruses by Host*
740 *Proteases*. Springer, Cham, p.205-248. Review.

741 Gierer S, Müller MA, Heurich A, Ritz D, Springstein BL, Karsten CB, Schendzielorz A, Gnirß K,
742 Drost C, Pöhlmann S. 2015. Inhibition of proprotein convertases abrogates processing of the middle
743 eastern respiratory syndrome coronavirus spike protein in infected cells but does not reduce viral
744 infectivity. *J Infect Dis* 211:889-97.

745 Hammami M, Rühmann E, Maurer E, Heine A, Gütschow M, Klebe G, Steinmetzer T. 2012. New 3-
746 amidinophenylalanine-derived inhibitors of matriptase. *MedChemComm* 3:807-13.

747 Hardes K, Becker GL, Lu Y, Dahms SO, Köhler S, Beyer W, Sandvig K, Yamamoto H, Lindberg I,
748 Walz L, von Messling V, Than ME, Garten W, Steinmetzer T. 2015. Novel furin inhibitors with potent
749 anti-infectious activity. *ChemMedChem* 10:1218-31.

750 Hardes K, Zouhir Hammamy M, Steinmetzer T. 2013. Synthesis and characterization of novel
751 fluorogenic substrates of coagulation factor XIII-A. *Anal Biochem* 442:223-30.

752 Hatesuer B, Bertram S, Mehnert N, Bahgat MM, Nelson PS, Pöhlmann S, Schughart K. 2013.
753 Tmprss2 is essential for influenza H1N1 virus pathogenesis in mice. *PLoS Pathog* 9:e1003774.

754 Heald-Sargent T, Gallagher T. Ready, set, fuse! 2012. The coronavirus spike protein and acquisition
755 of fusion competence. *Viruses* 4:557-80.

756 Hierholzer JC, Killington RA. 1996. Virus Isolation and Quantitation. In: Mahy BWJ, Kangro HO, (eds).
757 *Virology Methods Manual*. London, San Diego: Academic Press. pp. 24–32.

758 Hoffmann M, Hofmann-Winkler H, Pöhlmann S. 2018. Priming Time: How Cellular Proteases Arm
759 Coronavirus Spike Proteins. In: Böttcher-Friebertshäuser E., Garten W., Klenk H. (eds) *Activation of*
760 *Viruses by Host Proteases*. Springer, Cham, p.71-98. Review.

761 Hoffmann M, Kleine-Weber H, Schroeder S, Krüger N, Herrler T, Erichsen S, Schiergens TS, Herrler
762 G, Wu NH, Nitsche A, Müller MA, Drost C, Pöhlmann S. 2020. SARS-CoV-2 Cell Entry Depends on
763 ACE2 and TMPRSS2 and Is Blocked by a Clinically Proven Protease Inhibitor. *Cell*. pii: S0092-
764 8674(20)30229-4.

765 Iwata-Yoshikawa N, Okamura T, Shimizu Y, Hasegawa H, Takeda M, Nagata N. 2019. TMPRSS2
766 Contributes to Virus Spread and Immunopathology in the Airways of Murine Models after Coronavirus
767 Infection. *J Virol* 93:e01815-18.

768 Kacprzak MM, Peinado JR, Than ME, Appel J, Henrich S, Lipkind G, Houghten RA, Bode W, Lindberg
769 I. 2004. Inhibition of furin by polyarginine-containing peptides: nanomolar inhibition by nona-D-
770 arginine. *J Biol Chem* 279:36788-94.

771 Kassell B, Radicevic M, Ansfield MJ, Laskowski M. 1965. The basic trypsin inhibitor of bovine
772 pancreas. IV. The linear sequence of the 58 amino acids. *Biochem. Biophys. Res. Commun* 18: 255-8.

773 Kawase M, Shirato K, van der Hoek L, Taguchi F, Matsuyama S. 2012. Simultaneous treatment of
774 human bronchial epithelial cells with serine and cysteine protease inhibitors prevents severe acute
775 respiratory syndrome coronavirus entry. *J Virol* 86:6537-45.

776 Kim TS, Heinlein C, Hackman RC, Nelson PS. 2006. Phenotypic analysis of mice lacking the
777 Tmprss2-encoded protease. *Mol Cell Biol* 26:965-75.

778 Klenk HD, Garten W. 1994. Host cell proteases controlling virus pathogenicity. *Trends Microbiol* 2:39-
779 43.

780 Krüger N, Sauder C, Hutt S, Papies J, Voigt K, Herrler G, Hardes K, Steinmetzer T, Orvell C, Drexler
781 JF, Drosten C, Rubin S, Müller MA, Hoffmann M. 2018. Entry, Replication, Immune Evasion, and
782 Neurotoxicity of Synthetically Engineered Bat-Borne Mumps Virus. *Cell reports* 25:312-20.

783 Lai SH, Stein DA, Guerrero-Plata A, Liao SL, Ivanciu T, Hong C, Iversen PL, Casola A, Garofalo RP.
784 2008. Inhibition of Respiratory Syncytial Virus Infections with Morpholino Oligomers in Cell Cultures
785 and in Mice. *Molecular Therapy* 16:1120-8.

786

787 Limburg H, Harbig A, Bestle D, Stein DA, Moulton HM, Jaeger J, Janga H, Hardes K, Koepke J,
788 Schulte L, Koczulla AR, Schmeck B, Klenk HD, Böttcher-Friebertshäuser E. 2019. TMPRSS2 Is the
789 Major Activating Protease of Influenza A Virus in Primary Human Airway Cells and Influenza B Virus in
790 Human Type II Pneumocytes. *J Virol* 93:pii: e00649-19.

791 Lu Y, Hardes K, Dahms SO, Böttcher-Friebertshäuser E, Steinmetzer T, Than ME, Klenk HD, Garten
792 W. 2015. Peptidomimetic furin inhibitor MI-701 in combination with oseltamivir and ribavirin efficiently
793 blocks propagation of highly pathogenic avian influenza viruses and delays high level oseltamivir
794 resistance in MDCK cells. *Antiviral Res* 120:89-100.

795 Lupfer C, Stein DA, Mourich DV, Tepper SE, Iversen PL, Pastey M. 2008. Inhibition of Influenza A
796 H3N8 Infections in Mice by Morpholino Oligomers. *Archives of Virology* 153:929-37.

797

798 Madu IG, Roth SL, Belouzard S, Whittaker GR. 2009. Characterization of a highly conserved domain
799 within the severe acute respiratory syndrome coronavirus spike protein S2 domain with characteristics
800 of a viral fusion peptide. *J Virol* 83:7411-21.

801 Matsuyama S, Shirato K, Kawase M, Terada Y, Kawachi K, Fukushi S, Kamitani W. 2018. Middle East
802 Respiratory Syndrome Coronavirus Spike Protein Is Not Activated Directly by Cellular Furin during
803 Viral Entry into Target Cells. *J Virol* 92:pii: e00683-18.

804 Meyer D, Sielaff F, Hammami M, Böttcher-Friebertshäuser E, Garten W, Steinmetzer T. 2013.
805 Identification of the first synthetic inhibitors of the type II transmembrane serine protease TMPRSS2
806 suitable for inhibition of influenza virus activation. *Biochem J* 452:331-43.

807 Midgley I, Hood AJ, Proctor P, Chasseaud LF, Irons SR, Cheng KN, Brindley CJ, Bonn R. 1994.
808 Metabolic fate of 14C-camostat mesylate in man, rat and dog after intravenous administration.
809 *Xenobiotica* 24:79-92.

810 Millet JK, Whittaker GR. 2015. Host cell proteases: Critical determinants of coronavirus tropism and
811 pathogenesis. *Virus Res* 202:120-34. Review.

812 Moulton HM, Moulton JD. 2010. Morpholinos and their peptide conjugates: therapeutic promise and
813 challenge for Duchenne muscular dystrophy. *Biochim Biophys Acta* 1798:2296-2303. Review.

814 Opriessnig T, Patel D, Wang R, Halbur PG, Meng XJ, Stein DA, Zhang YJ. 2011. Inhibition of Porcine
815 Reproductive and Respiratory Syndrome Virus Infection in Piglets by a Peptide-Conjugated
816 Morpholino Oligomer. *Antiviral Research* 91:36-42.

817

818 Park JE, Li K, Barlan A, Fehr AR, Perlman S, McCray PB Jr, Gallagher T. 2016. Proteolytic processing
819 of Middle East respiratory syndrome coronavirus spikes expands virus tropism. *Proc Natl Acad Sci U
820 S A* 113:12262-7.

821 Rensi S, Altman RB, Liu T, Lo YC, McInnes G, Derry A, Keys A. Homology Modeling of TMPRSS2
822 Yields Candidate Drugs That May Inhibit Entry of SARS-CoV-2 into Human.
823 <https://chemrxiv.org/articles/Homolog> (preprint submitted on 20.03.2020)

824 Rockwell NC, Krysan DJ, Komiyama T, Fuller RS. 2002. Precursor processing by kex2/furin
825 proteases. *Chem Rev* 102:4525-48. Review.

826 Sakai K, Ami Y, Tahara M, Kubota T, Anraku M, Abe M, Nakajima N, Sekizuka T, Shirato K, Suzuki Y,
827 Arai A, Nakatsu Y, Kanou K, Nakamura K, Suzuki T, Komase K, Nobusawa E, Maenaka K, Kuroda

828 M, Hasegawa H, Kawaoka Y, Tashiro M, Takeda M. 2014. The host protease TMPRSS2 plays a major
829 role in in vivo replication of emerging H7N9 and seasonal influenza viruses. *J Virol* 88:5608-16.

830 Sarac MS, Cameron A, Lindberg I. 2002. The furin inhibitor hexa-D-arginine blocks the activation of
831 *Pseudomonas aeruginosa* exotoxin A in vivo. *Infect Immun* 70:7136-9.

832 Sarac MS, Peinado JR, Leppla SH, Lindberg I. 2004. Protection against anthrax toxemia by hexa-D-
833 arginine in vitro and in vivo. *Infect Immun* 72:602-5.

834 Shirato K, Kanou K, Kawase M, Matsuyama S. 2016. Clinical Isolates of Human Coronavirus 229E
835 Bypass the Endosome for Cell Entry. *J Virol* 91:pii: e01387-16.

836 Shirato K, Kawase M, Matsuyama S. 2013. Middle East respiratory syndrome coronavirus infection
837 mediated by the transmembrane serine protease TMPRSS2. *J Virol* 87:12552-61.

838 Shirato K, Kawase M, Matsuyama S. 2018. Wild-type human coronaviruses prefer cell-surface
839 TMPRSS2 to endosomal cathepsins for cell entry. *Virology* 517:9-15.

840 Simmons G, Gosalia DN, Rennekamp AJ, Reeves JD, Diamond SL, Bates P. 2005. Inhibitors of
841 cathepsin L prevent severe acute respiratory syndrome coronavirus entry. *Proc Natl Acad Sci U S A*.
842 102:11876-81.

843 Singh S, Khaytin I, Botsko S, Crossley G, Plank DK, Lefievre Y, Giuffrida F. 2002. Pennington, M. W.
844 Addition of o-aminobenzoic acid during Fmoc solid phase synthesis of a fluorogenic substrate
845 containing 3-nitrotyrosine. *Letters in Peptide Science* 9:221-5.

846

847 Stein DA. 2008. Inhibition of RNA virus infections with peptide-conjugated morpholino oligomers. *Curr*
848 *Pharm Des* 14:2619-34.

849 Steinmetzer T, and Hardes, K. 2018. The Antiviral Potential of host protease inhibitors. In: Böttcher-
850 Friebertshäuser E., Garten W., Klenk H. (eds) Activation of Viruses by Host Proteases. Springer,
851 Cham, p.279-325. Review.

852 Steinmetzer T, Pilgram O, Wenzel BM, Wiedemeyer SJA. 2020. Fibrinolysis Inhibitors: Potential Drugs
853 for the Treatment and Prevention of Bleeding. *J Med Chem* 63:1445-72.

854 Tanaka N, Tsuchiya R, Ishii K. 1979. Comparative clinical study of FOY and Trasylol in acute
855 pancreatitis. *Adv Exp Med Biol* 120B:367-78.

856 Tarnow C, Engels G, Arendt A, Schwalm F, Sediri H, Preuss A, Nelson PS, Garten W, Klenk HD,
857 Gabriel G, Böttcher-Friebertshäuser E. 2014. TMPRSS2 is a host factor that is essential for
858 pneumotropism and pathogenicity of H7N9 influenza A virus in mice. *J Virol* 88:4744-51.

859 Van Lam van T, Ivanova T, Hardes K, Heindl MR, Morty RE, Böttcher-Friebertshäuser E, Lindberg I,
860 Than ME, Dahms SO, Steinmetzer T. 2019. Design, Synthesis, and Characterization of Macrocyclic
861 Inhibitors of the Proprotein Convertase Furin. *ChemMedChem* 14:673-85.

862 Walls AC, Park YJ, Tortorici MA, Wall A, McGuire AT, Veesler D. 2020. Structure, Function, and
863 Antigenicity of the SARS-CoV-2 Spike Glycoprotein. *Cell*. pii: S0092-8674(20)30262-2.

864 Walls AC, Tortorici MA, Bosch BJ, Frenz B, Rottier PJM, DiMaio F, Rey FA, Veesler D. 2016. Cryo-
865 electron microscopy structure of a coronavirus spike glycoprotein trimer. *Nature* 531:114-7.

866 Watanabe R, Matsuyama S, Shirato K, Maejima M, Fukushi S, Morikawa S, Taguchi F. 2008. Entry
867 from the cell surface of severe acute respiratory syndrome coronavirus with cleaved S protein as
868 revealed by pseudotype virus bearing cleaved S protein. *J Virol* 82:11985-91.

869 Zhirnov OP, Klenk HD, Wright PF. 2011. Aprotinin and similar protease inhibitors as drugs against
870 influenza. *Antiviral Res* 92:27-36.

871 Zhou Y, Vedantham P, Lu K, Agudelo J, Carrion R Jr, Nunneley JW, Barnard D, Pöhlmann S,
872 McKerrow JH, Renslo AR, Simmons G. 2015. Protease inhibitors targeting coronavirus and filovirus
873 entry. *Antiviral Res* 116:76-84.

Figure 1

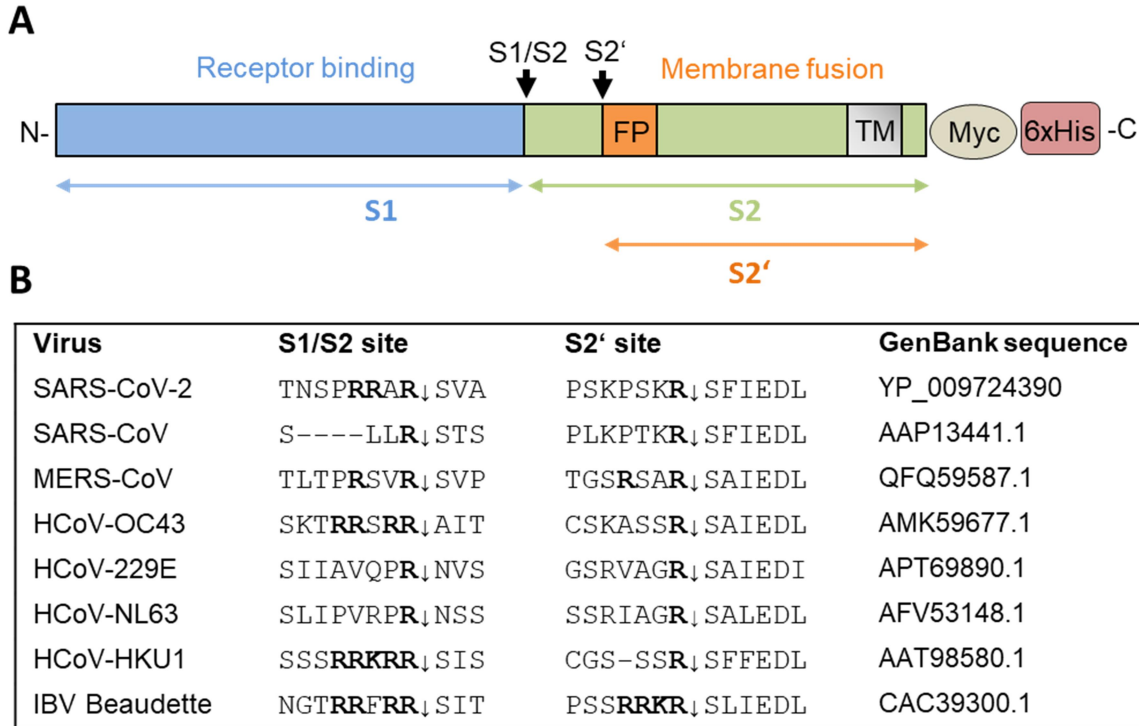


Figure 1: Cleavage of coronavirus S protein. A) Schematic representation of the SARS-CoV-2 precursor and the S1 and S2 subunits. Fusion peptide (FP), transmembrane domain (TM). The S1/S2 and S2' cleavage sites and subunits S1, S2 and S2' are indicated by black and coloured arrows, respectively. For immunochemical detection recombinant S is expressed with a C-terminally fused Myc-6xHis-tag peptide in our study. **B)** Alignment of the amino acid sequences at the S1/S2 and S2' cleavage site of the S proteins of different human coronaviruses (HCoV) and avian infectious bronchitis virus (IBV) strain Beaudette.

Figure 2

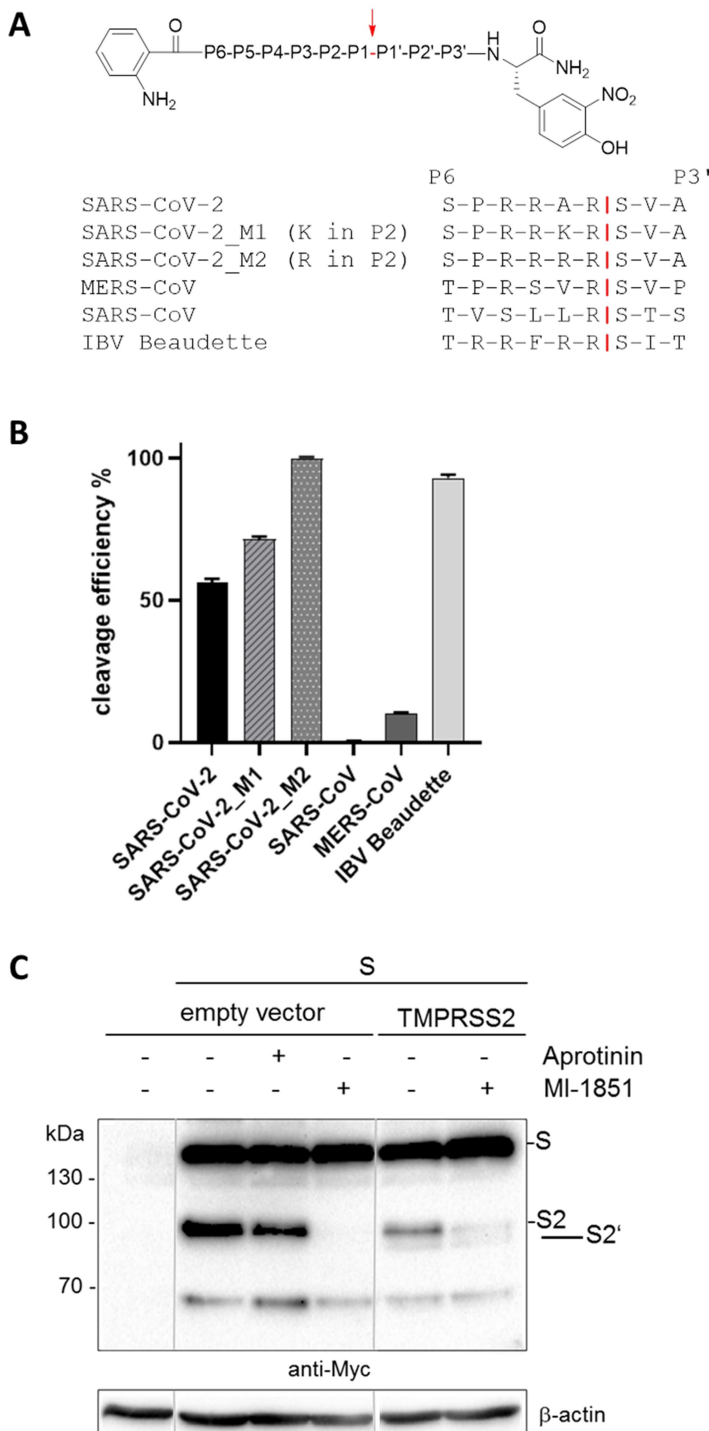


Figure 2: Cleavage of SARS-CoV-2 S by furin and TMPRSS2. A) FRET substrates of the S protein S1/S2 sites of the indicated CoVs. M1 and M2 are mutants of the SARS-CoV-2 S1/S2 site with substitution of A→K or A→R in P2 position. IBV: avian infectious bronchitis virus strain Beaudette. Cleavage by furin is indicated in red. **B)** Cleavage of the FRET substrates (20 μ M) by furin (0.5 nM). Cleavage efficiency of SARS-CoV-2_M2 was set as 100 %. **C)** Cleavage of SARS-CoV-2 S by furin and TMPRSS2 in HEK293 cells. Cells were

co-transfected with pCAGGS-S-Myc-6xHis and either empty vector or pCAGGS-TMPRSS2. Cells were then incubated in the absence or presence of aprotinin or furin inhibitor MI-1851 (50 μ M each) for 48 h. Cell lysates were subjected to SDS-PAGE and Western blot analysis using antibodies against the C-terminal Myc-tag. Lanes are spliced together from one immunoblot from one experiment.

Figure 3

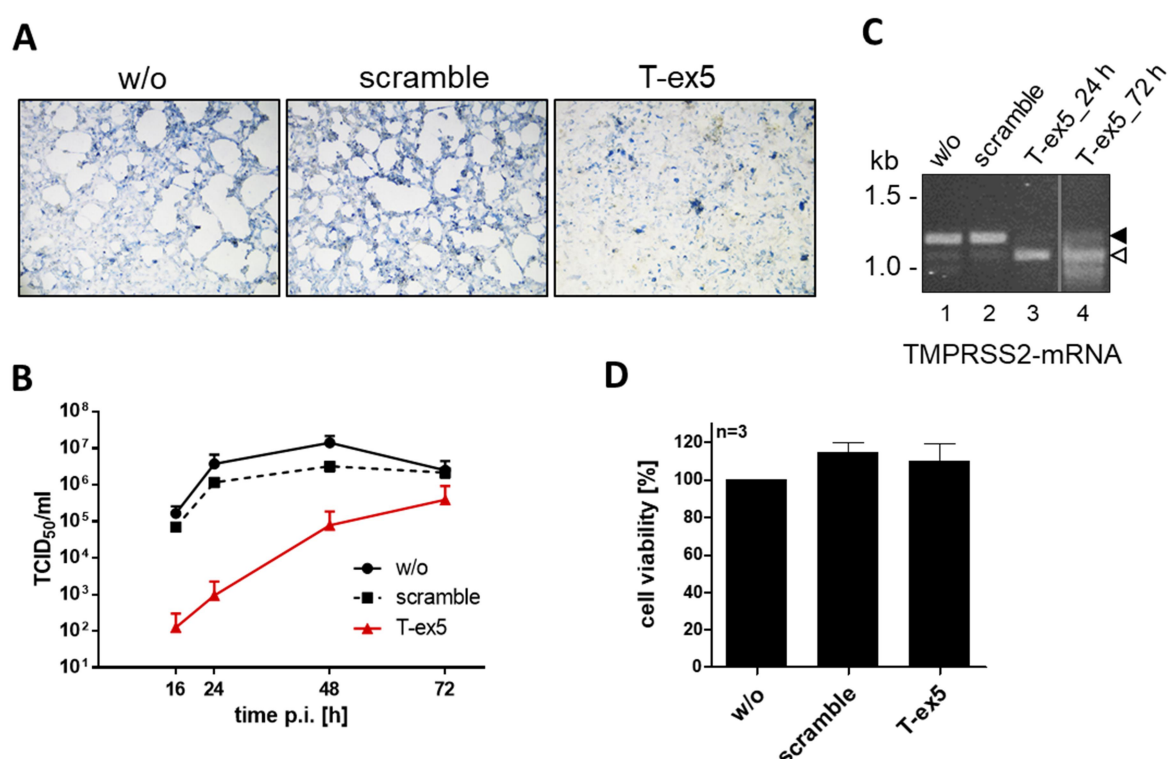


Figure 3: Knockdown of TMPRSS2 expression by PPMO T-ex5 inhibits multicycle replication of SARS-CoV-2 in Calu-3 cells. A) Multicycle replication of SARS-CoV-2 in T-ex5 treated Calu-3 cells. Cells were treated with 25 μ M T-ex5 or control PPMO (scramble) for 24 h or remained untreated (w/o), then inoculated with SARS-CoV-2 at a MOI of 0.001 and further incubated in the absence of PPMO for 72 h. Cells were fixed and immunostained using a serum against SARS-CoV. **B)** Calu-3 cells were treated with PPMO for 24 h and then infected with SARS-CoV-2 for 72 h as described above. Virus titers in supernatants were determined by tissue culture infection dose 50 % (TCID₅₀) end-point dilution at indicated time points. Results are mean values \pm standard deviations (SD) of two independent experiments (n=2). **C)** Analysis of TMPRSS2-mRNA in PPMO-treated Calu-3 cells. Cells were treated with 25 μ M T-ex5, scramble PPMO or remained untreated (w/o) for 24 h (lanes 1-4). T-ex5 treated cells were inoculated with SARS-CoV-2 as described above and incubated in the absence of PPMO for 72 h (lane 4). Total RNA was isolated and analysed by RT-PCR using primers designed to amplify 1228 nt of full-length TMPRSS2-mRNA. Full-length and truncated PCR product lacking exon 5 are indicated by filled and open arrow heads, respectively. **D)** Effect of PPMO treatment on Calu-3 cell viability. Calu-3 cells were treated with scramble or T-ex5 PPMO (25 μ M) for 24 h. Cell viability of untreated (w/o) cells was set as 100 %. Results are mean values \pm SD (n=3).

Figure 4

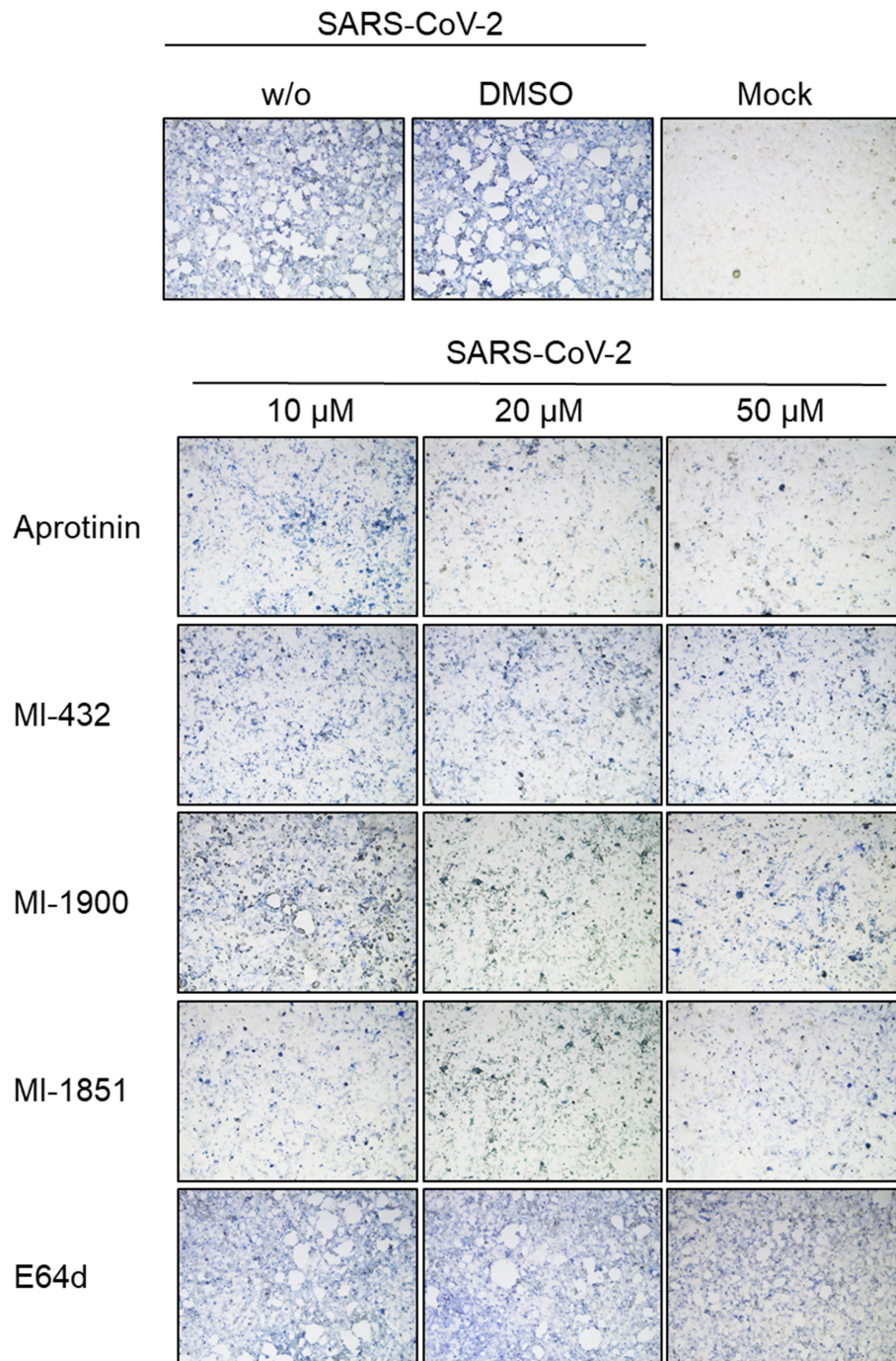


Figure 4: Inhibition of SARS-CoV-2 multiplication in human airway cells by inhibitors of furin and TMPRSS2. Calu-3 cells were inoculated with SARS-CoV-2 at a low MOI of 0.001 and then incubated in the presence of inhibitors of TMPRSS2 (aprotinin, MI-432, MI-1900), furin (MI-1851), and endosomal cathepsins (E64d), respectively, at the indicated concentrations. Cells were fixed and immunostained using a rabbit serum against 2002 SARS-CoV at 72 h post infection (p.i.). Cells infected in the absence of inhibitors (w/o), in the presence of DMSO (0.5 %) and non-infected cells (mock) were used as controls. Images are representatives of three independent experiments.

Figure 5

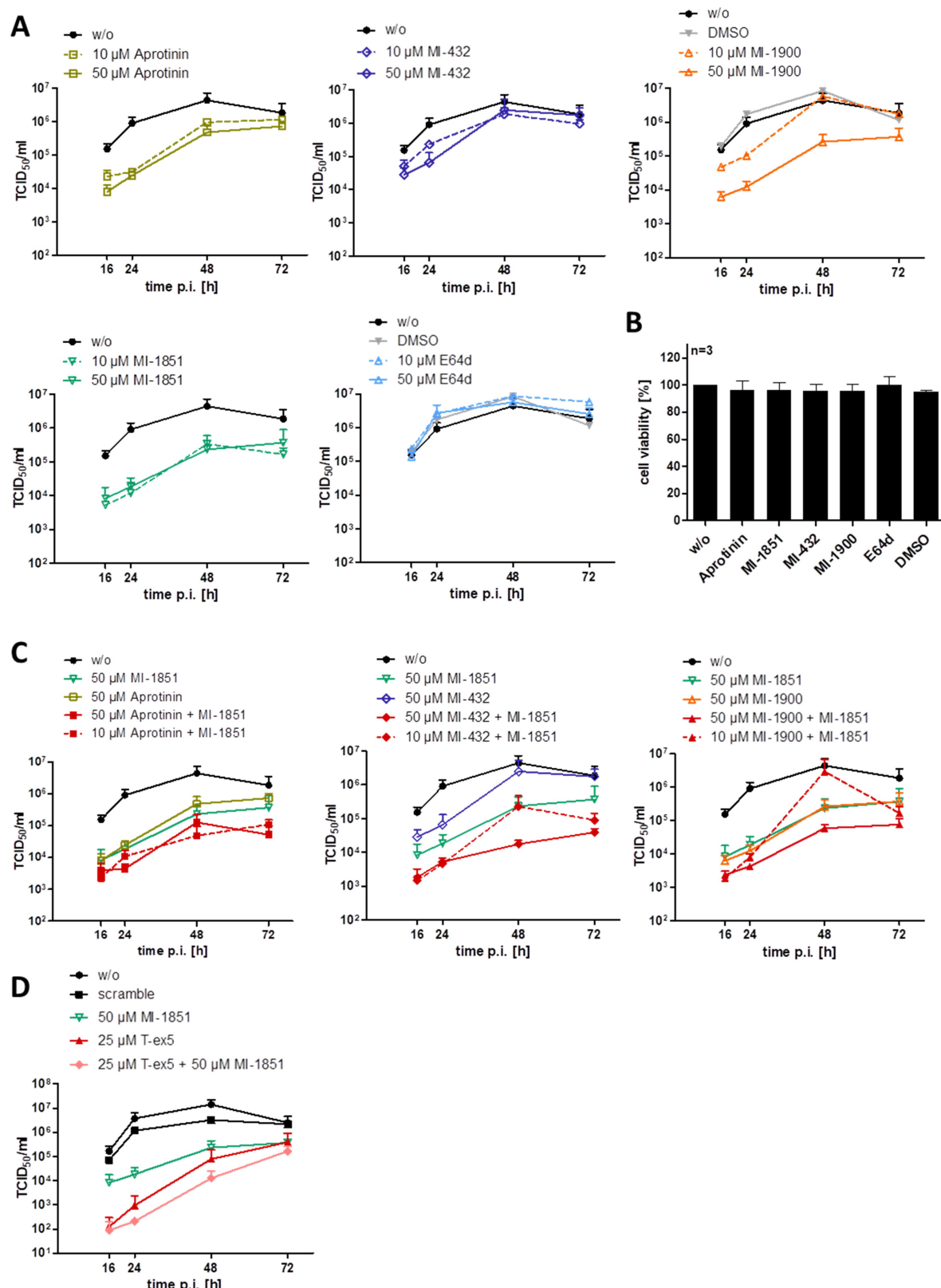


Figure 5: Inhibition of SARS-CoV-2 multicycle replication in human airway epithelial cells by inhibitors of TMPRSS2 and furin. A) Calu-3 cells were inoculated with SARS-CoV-2 at a low MOI of 0.001 and then incubated in the absence (w/o) or presence of

inhibitors of TMPRSS2 (aprotinin, MI-432, MI-1900), furin (MI-1851), and endosomal cathepsins (E64d), respectively, or DMSO (0.5 %), at the indicated concentrations. At 16, 24, 48, and 72 h p.i., supernatants were collected, and virus replication was determined by TCID₅₀ titration at indicated time points. Data are mean values \pm SD from two to four independent experiments. **B)** Effect of inhibitor treatment on cell viability. Calu-3 cells were treated with the indicated protease inhibitor (50 μ M) for 72 h. Untreated cells (w/o) and DMSO treated cells were used as controls. Cell viability of untreated cells was set as 100 %. Results are mean values \pm SD (n=3). **C)** Antiviral activity of combinations of TMPRSS2 and furin inhibitors against SARS-CoV-2 in human airway epithelial cells. Calu-3 cells were inoculated with SARS-CoV-2 at a MOI of 0.001 as described above and then incubated in the presence of single protease inhibitors or inhibitor combinations at the indicated concentrations. Virus titers in supernatants were determined by TCID₅₀ at 16, 24, 48 and 72 h p.i.. Data are mean values \pm SD of two to three independent experiments. **D)** Calu-3 cells were treated with PPMO for 24 h, then infected with SARS-CoV-2 as described above and incubated in the absence of PPMO (w/o, scramble and T-ex5) and with or without 10 μ M of furin inhibitor treatment (MI-1851) for 72 h. At 16, 24, 48, and 72 h p.i., supernatants were collected, and viral titers were determined by TCID₅₀ at indicated time points. Data are mean values \pm SD (n=2).

Figure 6

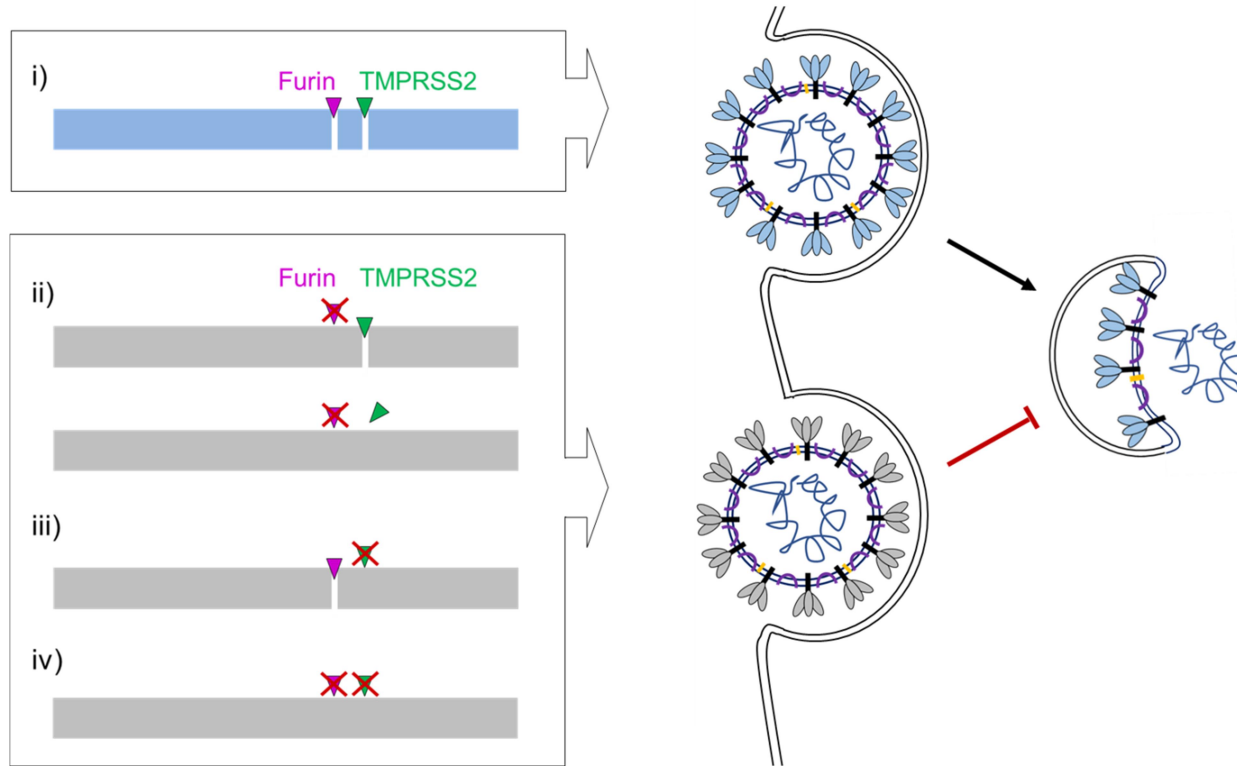
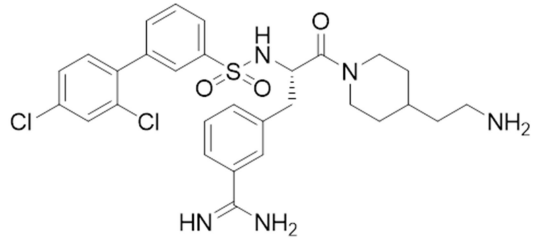


Figure 6: Proposed processing of SARS-CoV-2 spike protein S by TMPRSS2 and furin.

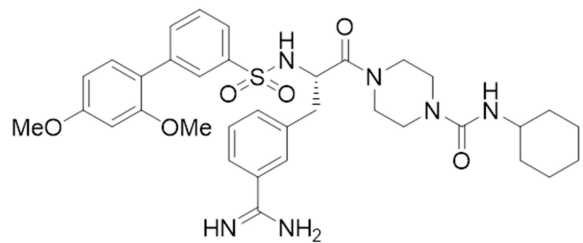
i) S must be cleaved at two sites, S1/S2 and S2', to trigger fusion of viral and cellular membranes during virus entry in order to release the virus genome into the host cell. CoV S cleavage is believed to occur sequentially, with cleavage at the S1/S2 site occurring first and subsequent cleavage at the S2' site. Furin processes the S1/S2 site, whereas TMPRSS2 cleaves at the S2' site, and both proteases cannot compensate each other. Inhibition of either furin (ii) or TMPRSS2 (iii) or simultaneous inhibition of both proteases (iv) renders the S protein fusion-inactive and prevents virus entry. Inhibition of TMPRSS2 prevents exposure of the fusion peptide at the N-terminus of the S2' subunit (iii and iv). Inhibition of furin cleavage at the S1/S2 site may directly interfere with virus entry and membrane fusion by steric blockage of conformational changes (ii, upper scheme) or may prevent exposure of the S2' site to TMPRSS2 (ii, lower scheme). Fusion-competent S is indicated in blue, fusion-incompetent S in grey.

Figure S1

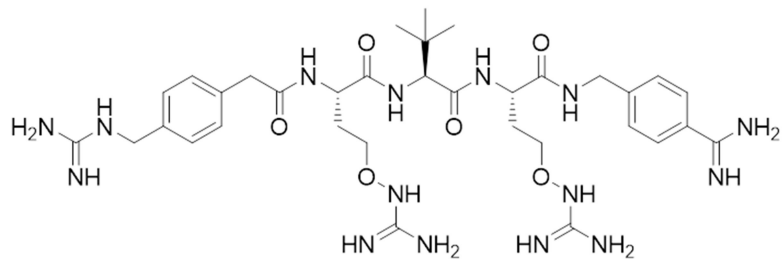
MI-432



MI-1900



MI-1851



Aprotinin

RPDFCLEPPYTGPCKARIIRYFYNAKAGLCQTFVYGGCRAKRNNFKSAEDCMRTCGGA

Figure S1: Structural formulas of peptide mimetic inhibitors MI-432, MI-1900 and MI-1851 and the linear amino acid sequence of bovine aprotinin (Kassell et al., 1965).

Figure S2

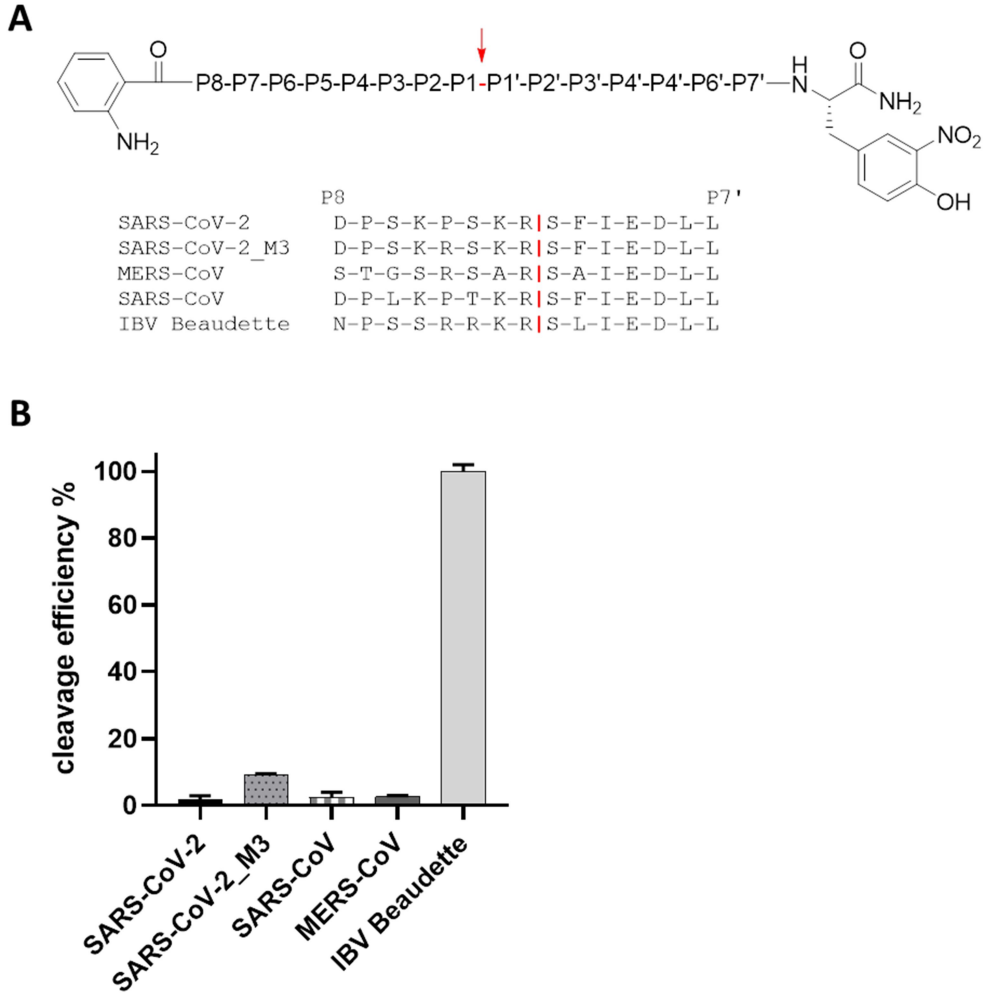


Figure S2: Cleavage analysis of SARS-CoV-2 S2' site by furin. **A)** FRET substrates of the S protein S2' sites of the indicated CoVs. M3 is a mutant of the SARS-CoV-2 S2' site with substitution of P→R in P4 position. IBV: avian infectious bronchitis virus strain Beaudette. Cleavage by furin is indicated in red. **B)** Cleavage of the FRET substrates (20 μ M) by furin (0.5 nM). Cleavage efficiency of IBV Beaudette was set as 100%.